



Sources, concentrations, and seasonal variations of VOC and aerosol particles in downtown Munich in 2023/24

- ³ Yanxia Li¹, Hengheng Zhang^{1,a}, Xuefeng Shi¹, Yaowei Li^{2,b}, Sophie Abou-Rizk², Jessica B.
- 4 Smith², Zhaojin An^{2,c}, Adrian Wenzel³, Junwei Song⁴, Thomas Leisner^{1,5}, Frank Keutsch², Jia
- 5 Chen³, and Harald Saathoff¹
- 6 ¹Institute of Meteorology and Climate Research-Atmospheric Aerosol Research, Karlsruhe Institute of
- 7 Technology, 76344 Eggenstein-Leopoldshafen, Germany
- 8 Paulson School of Engineering and Applied Sciences, Harvard University, Cambridge, MA 02138, USA
- ³Environmental Sensing and Modeling, Technical University of Munich (TUM), Munich, Germany
- 4Irceylon, Universite Claude Bernard Lyon 1, CNRS, UMR 5256, Villeurbanne, 69100, France
- ⁵Institute of Environmental Physics, Heidelberg University, 69120 Heidelberg, Germany
- ^anow at: Research Institute for Applied Mechanics, Kyushu University, Fukuoka, Japan
- 13 bnow at: Department of Earth, Atmospheric, and Planetary Sciences, Massachusetts Institute of Technology,
- 14 Cambridge, MA 02139, USA

16

- 15 cnow at: School of Environment, Tsinghua University, 10084, Beijing China
- 17 Corresponding authors: Yanxia Li (yanxia.li@kit.edu) and Harald Saathoff (Harald.Saathoff@kit.edu)
- Abstract. Only little is known about molecular composition and sources of air pollution in Germany's third largest
- 19 city, Munich. Therefore, we investigated sources, concentrations, and seasonal variations of volatile organic
- 20 compounds (VOC), semi-volatile organic aerosol (SVOA), and organic aerosol (OA) in an urban street canyon in
- 21 Munich utilizing online mass spectrometry and positive matrix factorization (PMF). Organic aerosol
- 22 concentrations were higher in summer $(4.3 \pm 2.9 \ \mu g \ m^{-3})$ than late winter $(3.3 \pm 1.7 \ \mu g \ m^{-3})$ due to enhanced
- photochemical reactions, while nitrate exhibited the opposite trend with elevated concentrations in winter (4.5 \pm
- $3.2 \,\mu g \, m^{-3}$) compared to summer $(0.3 \pm 0.2 \,\mu g \, m^{-3})$. During summer heat, photochemistry generates low-volatile
- oxygenated OA (33 \pm 20%), while aged biomass burning organic aerosol (BBOA) (25 \pm 21%) from barbecue
- activities and biogenic OA (22 \pm 14%) from nocturnal monoterpene chemistry further shape aerosol composition.
- The colder seasons are characterized by combustion-derived aerosols (Winter: fresh BBOA $13 \pm 9\%$, aged $36 \pm 9\%$), aged $36 \pm 9\%$
- 12%; Spring: fresh $27 \pm 17\%$, aged $37 \pm 19\%$), whose dynamics are driven mainly by anthropogenic activity
- 29 patterns. Traffic contributed at this urban kerbside surprisingly little to aerosol mass (5-9 %) but more to VOC
- 30 (22-35%). Our findings point to efficient ways to improve air quality e.g. by reducing monoterpene emissions by
- 31 urban vegetation management as well as reducing biomass burning including barbecue emissions, a major source
- 32 of aerosol particles and precursor gases of secondary organic aerosol throughout the seasons.

1. Introduction

33

- Volatile organic compounds (VOC) and organic aerosols (OA) are major components of urban air pollution,
- 35 contributing to the formation of secondary pollutants like ozone and secondary organic aerosol (SOA), which
- pose significant risks to air quality, climate, and human health (Wu et al., 2020; Nault et al., 2021; Ipcc, 2023).
- 37 Moreover, different weather conditions and seasons influence the dispersion, deposition, and transformation of
- these pollutants (Crippa et al., 2013; Debevec et al., 2021; Stirnberg et al., 2021). Identifying SOA sources is
- crucial for reducing complex observational datasets to key real-world contributors, enabling timely air quality





40 management, policy evaluation, and accurate air pollution forecasting (Chen et al., 2022a). However, pinpointing the sources of SOA is particularly challenging due to its composition as a highly complex mixture of largely 41 unidentified compounds, coupled with the complicated and multistep transformation processes of VOC into SOA 42 (Daellenbach et al., 2019). 43 44 The high-resolution time-of-flight Aerodyne aerosol mass spectrometer (HR-TOF-AMS) is commonly used for the online characterization of non-refractory PM_{2.5}. AMS datasets combined with positive matrix factorization 45 (PMF) analysis can quantitatively identify major primary organic aerosol (POA) sources, including traffic-related 46 hydrocarbon-like organic aerosol (HOA) and biomass burning organic aerosol (BBOA) (Chakraborty et al., 2017; 47 48 Lalchandani et al., 2021). However, AMS datasets cannot specify sources for secondary organic aerosol (SOA) due to significant fragmentation from thermal volatilization (~600°C) and harsh electron impact ionization (~70 49 eV) (Qi et al., 2020; Kumar et al., 2022). Additionally, without information on VOC as SOA precursors, it is 50 51 difficult to attribute SOA factors (e.g., semi-volatile oxygenated OA (SV-OOA) and low-volatility oxygenated OA (LV-OOA)) to specific sources or formation mechanisms using AMS-PMF analysis (Song et al., 2024). 52 Proton transfer reaction time-of-flight mass spectrometry (PTR-TOF-MS) is a useful tool to identify the sources 53 of VOC and oxygenated VOC (OVOC), and in elucidating their contributions to the SOA formation (Wang et al., 54 2020a; Pfannerstill et al., 2019). Furthermore, the CHARON-PTR-MS (Chemical Analysis of Aerosol Online 55 Particle Inlet coupled to a PTR-TOF-MS) is a continuous measurement technique capable of qualitatively and 56 quantitatively detecting semi-volatile organic aerosol particles (Eichler et al., 2015; Muller et al., 2017; Piel et al., 57 2019). CHARON-PTR-MS enhances the detection of detailed SOA chemical composition data by minimizing 58 thermal decomposition and ionization-induced fragmentation, providing more information on identifying SOA 59 sources compared to AMS (Gkatzelis et al., 2018b; Leglise et al., 2019). 60 Huang et al. (2019) found that in the city of Stuttgart (southwest Germany) SOA from VOC oxidation dominated 61 62 the organic aerosol burden, with primary sources like traffic contributing less, while residential wood burning became particularly important during winter in residential areas. A study in the downtown of the city of Karlsruhe 63 (southwest Germany) demonstrated that secondary oxygenated OA comprised over 60-75% of total OA 64 throughout the year, with primary traffic-related OA showing seasonal variations and wood combustion becoming 65 66 more significant during cold periods under stagnant meteorological conditions (Song et al., 2022). A Europe-wide analysis revealed that oxygenated OA (secondary formation) accounted for an average of 71% of submicron OA 67 mass across 22 sites, with solid fuel/biomass burning contributing 16% and primary urban sources (traffic, 68 69 cooking) typically less than 10-15% (Chen et al., 2022b). These findings underscore the necessity for site-specific OA and VOC source apportionment studies in major European cities such as Munich in southern Germany, while 70 secondary formation processes consistently dominate regional OA burdens, the underlying VOC precursors, and 71 72 primary emission contributions exhibit substantial spatial and temporal variability. 73 Munich, the capital of Bavaria, Germany, is a major cultural and economic center with a population of 1.5 million as of 2023, making it the third-largest city in Germany. It has a population density of 4,700 people per square 74 kilometers (München, 2023). Despite significant progress in air quality regulations, Munich still struggles with 75 76 aerosol pollution. Identifying the sources of VOC and particulate matter is crucial for improving air quality in Munich. However, there have been only a limited number of studies characterizing aerosols in Munich. Schnelle-77 Kreis J. et al. (2001) collected filters from three traffic-dominated sites and one additional site located on the 78 79 northern outskirts of Munich, approximately 1 km from the city center, between 1996 and 1998. Using HPLC



81

82

83 84

85

86

87 88

89

90 91

92

93 94

95

96 97

98

99

100 101

102

103

104

106

107

108 109

110

111

112

113



analysis, they found that 40% of polycyclic aromatic hydrocarbons (PAHs) were associated with fine particles. Schäfer et al. (2011) monitored air pollution across Munich and its outskirts, employing long-term as well as campaign-based monitoring stations from LfU (Bayerisches Landesamt Für Umwelt), Meteorological Institute of the Ludwig-Maximilians-University Munich (MIM), and IMK-IFU (e.g., Maisach) covering traffic-related (e.g., Lothstraße, Stachus, Luise-KiesselbachPlatz), urban (MIM), and suburban (Johanneskirchen) sites, during campaigns in late spring (10th-30th May 2003) and winter (27th November-15th December 2003). They found higher particle mass concentrations at the urban site compared to rural areas, especially in winter, with no significant differences in major ionic composition between the sites (Schäfer et al., 2011). Qadir et al. (2013) identified traffic, cooking, solid fuel combustion, and mixed aerosols (from tobacco smoke, cooking, and wood combustion) as the primary sources of aerosols at Lothstraße in Munich during the winter periods of October 2006 to February 2007 and October 2009 to February 2010. Schnell (2014) identified biomass burning aerosol as the dominant aerosol type at the rural site of Maisach and the urban site of MIM during the winter seasons from 2007 to 2010. Recently, a study on aerosol emissions from Munich Airport showed its impact in the outskirts of Munich, especially for ultrafine particles (UFPs) (Seidler et al., 2024). Despite these previous studies, we still have limited understanding of the main sources of VOC and OA through concurrent online measurements, their typical concentration levels across seasons, and their seasonal variations in molecular composition in Munich. It remains unclear how much anthropogenic and biogenic sources contribute to air pollution in Munich and what is the fraction of wood combustion vs. barbeque for biomass burning aerosol. Therefore, we examined in this study the seasonal variability of OA and VOC chemical composition at a molecular level in a street canyon (Theresienstrasse 39) in downtown Munich, aiming to elucidate the contribution of different sources to major VOC, SVOA, and total OA concentrations. The PM_{2.5} concentrations at the Theresienstrasse are comparable to those observed at the regulatory monitoring station Munich/Stachus of LfU. For 2023, the annual average PM_{2.5} concentration at the reference station was $9.3 \pm 6.2 \,\mu g \, m^{-3}$, with August showing $8.7 \pm 5.7 \,\mu g \, m^{-3}$, compared to our measured value of $6.7 \pm 3.7 \ \mu g \ m^{-3}$. In 2024, the annual average at the reference station was $8.7 \pm 6.6 \ \mu g \ m^{-3}$, with March averaging $9.0 \pm 9.9 \,\mu g$ m⁻³, while our March measurements yielded $8.7 \pm 9.2 \,\mu g$ m⁻³. Both measurement periods demonstrated strong correlations (R=0.8) (Figure S1). The close agreement between our measurements and the official monitoring data, combined with the high correlation coefficients, validates the representativeness of our sampling location for characterizing the urban downtown atmosphere in Munich. Please note that this work is linked to the recently established low-cost sensor network in downtown Munich, monitoring especially O₃, NO₂, and PM_{2.5} (Wenzel et al., 2025). For our dedicated source apportionment, we conduct separate statistical analyses on VOC from PTR-TOF-MS, SVOA from CHARON-PTR-MS, and OA from HR-TOF-AMS to identify the sources of VOC, SVOA, and OA from their chemical fingerprints.

2. Methodology

2.1 Measurement location

Field observations were conducted during three distinct seasons: summer (3rd-29th August 2023), late winter (1st-8th March 2024), and spring (9th-27th March 2024). The separation between winter and spring periods was based on ambient temperature trends and nitrate concentrations. The sampling site (11°57'E, 48°15'N) was located on a parking lot next to a 30 m tall building of the Ludwigs-Maximilians-University (LMU) of Munich in a street





canyon of Theresienstrasse 39 (Figure S2). The elevation on street level at this location is 520 m a.s.l. The street has several restaurants, apartment buildings, museums, university workshops, laboratories, and substantial vehicular traffic. The wind direction at the site in the street canyon predominantly originates from the south and southeast due to a vortex due to upwind or lee side of the LMU building. At the rooftop of the 30-meter LMU building, it mainly came from the west and east. Wind speed and direction exhibit minimal variation for the measurement periods (Figure S2).

2.2 Instrumentation

124

125

126

127

154

155

An overview of all instruments used in this campaign to characterize aerosol particles, trace gases, and meteorological parameters is provided in Table S1. The major instruments used are described in more detail below.

2.2.1 CHARON-PTR-TOF-MS

A proton-transfer-reaction time-of-flight mass spectrometer (PTR-ToF-MS 4000X2, Ionicon Analytik GmbH), 128 129 equipped with a particle inlet (Chemical Analysis of aeRosol ONline, CHARON), was utilized to measure VOC in the gas phase and semi-volatile compounds in the particle phase. The PTR-ToF-MS 4000X2 employed here 130 131 has an ion funnel, which reduces ion loss and enhances sensitivity (Pugliese et al., 2020). The CHARON inlet 132 integrates a gas-phase denuder, an aerodynamic lens with an inertial sampler, and a thermo-desorption unit, all coupled to a PTR-TOF-MS. The gas-phase denuder removes gas-phase analytes, while the aerodynamic lens 133 focuses the aerosol particles. The inertial sampler then concentrates the particle-enriched sample flow. Finally, 134 135 the particles enter a thermal desorption unit where they are volatilized before being detected by PTR-MS. The inlet system demonstrated a particle enrichment factor of 18 ± 2 (Figure S3), as discussed in detail in our previous 136 study (Song et al., 2024). The vaporizer (TDU) was operated at 150 °C and 7-8 mbar absolute pressure. The 137 CHARON inlet was described in detail elsewhere (Eichler et al., 2015; Muller et al., 2017; Gkatzelis et al., 2018a; 138 Gkatzelis et al., 2018b). 139 140 In this campaign, the CHARON-PTR-MS automatically switched between gas and particle phase measurements. The sequence was: 5 minutes of high-efficiency particulate air (HEPA) filter measurement for particle background, 141 10 minutes of particle-phase measurement, 3 minutes transition, 10 minutes of gas-phase VOC measurement, and 142 143 another 2 minutes transition. The PTR drift tube was kept at 2.7 mbar, 470 V, and 100 °C, with the ion funnel at 144 45 V. These settings correspond to an electric field (E) to gas molecule number density (N) ratio of ~100 Td for VOC measurement. For particle measurement, the PTR was automatically adjusted to 60 Td. 145 During gas-phase measurement, ambient air was sampled continuously from a 2 m PFA tube (4 mm inner diameter) 146 at 8 L/min, with 40-100 mL/min directed to the PTR-ToF-MS through a polyetheretherketone (PEEK) tubing at 147 80°C. The gas background was manually measured weekly using pure nitrogen for 5-15 minutes. For particle-148 phase measurement, ambient particles were sampled with a PM_{2.5} inlet (Comde Dendra) through a vertical 149 150 electropolished 3.45 m stainless-steel tube (12 mm inner diameter) at 16.7 L/min, with 550 mL/min directed to the CHARON inlet. Particle background was automatically determined using the HEPA filter. 151 Gas calibrations were performed at the beginning, middle, and end of each campaign periods using a gas cylinder 152 (Ionicon Analytik GmbH) with 15 VOC, including toluene, trimethylbenzene, xylene, alpha-pinene, acetone, 153

acetonitrile, benzene, and isoprene (accuracy 5% at ~1000 ppb). The sensitivity ranged from ~1000 to 4000

cps/ppb for different compounds across different seasonal calibration periods (Figure S4). Raw data from





156 CHARON-PTR-MS were processed using IONICON Data Analyzer software (IDA 2.2.0) following Müller et al. (2013), Lannuque et al. (2023), and Peron et al. (2024). The CHARON inlet enrichment factor was determined via external calibration with size-selected (DMA, TSI) ammonium nitrate particles (100-500 nm) measured by a condensation particle counter (CPC, TSI).

2.2.2 HR-TOF-AMS

160

161

162 163

164

165

166 167

168

169

170 171

172

173 174

175

176 177

178

179 180

181

182

183

184

185

186

187 188

189

190

191

192

193

A high-resolution time-of-flight Aerosol Mass Spectrometer (HR-ToF-AMS) (Aerodyne Research Inc.), equipped with a PM2.5 aerodynamic lens, was used to measure non-refractory PM2.5 (NR-PM2.5) components, including organic aerosol, nitrate, sulfate, ammonium, and chloride, with a time resolution of 1 minute (Peter F. Decarlo et al., 2006; Canagaratna et al., 2007; Williams et al., 2013). The operation and calibration procedures of the AMS are detailed in our previous publications (Huang et al., 2019; Song et al., 2022). The instrument's capability to provide high-resolution mass spectra enables detailed chemical composition analysis of aerosol particles in real time. Briefly, ambient air was sampled through a PM_{2.5} inlet (flow rate of 1 m³ h⁻¹) that was shared with the CHARON system via a 3.45 m stainless-steel tube. A subset of this flow was then directed to the HR-ToF-AMS at a flow rate of 84 cm3 min-1. The aerosol particles were focused into a narrow beam by a PM2.5 aerodynamic lens, which effectively transmits particles with vacuum aerodynamic diameters (dva) ranging from ~70 to ~2500 nm. The particles were subsequently heated by a vaporizer at 600°C, causing the non-refractory components to volatilize. The volatilized particles were then ionized by electron impact at 70 eV, which is a standard method for ionizing organic and inorganic compounds, ensuring fragmentation patterns that are wellcharacterized and suitable for identification. The AMS was calibrated using ~300 nm dried ammonium nitrate aerosol particles to optimize lens transmission (70-500 nm) and ionization efficiency, with DMA selection and signal validation. The calibrations were done before and each measurement period. Data from the AMS were processed and analyzed using the SQUIRREL 1.65G and PIKA 1.25G software packages. To address the issue of particle bounce losses, a chemical-composition-based collection efficiency (CE) of approximately 0.5 was applied to calculate the particle mass concentrations (Docherty et al., 2011; Middlebrook et al., 2012). For the elemental analysis of organic aerosol (OA), including the hydrogen-to-carbon ratio (H: C) and the oxygen-to-carbon ratio (O: C), we utilized the improved ambient method (Allison C. Aiken et al., 2008; Canagaratna et al., 2015).

2.2.3 Other Instruments

The mass concentrations of $PM_{2.5}$ and PM_{10} and particle size distributions (0.2-18 µm) were determined using an optical particle counter (Fidas200, Palas). Particle number concentrations (> 2.5 nm) were monitored using a water-based condensation particle counter (Model 3789, TSI Inc.) and a butanol-based condensation particle counter CPC3776 (TSI Inc., USA). Particle number size distributions ranging from 10 to 410 nm were measured using a nanoparticle sizer (Nanoscan 3910; TSI Inc.) at time resolution of 1 min in winter, and distributions ranging from 13.6 to 763.5 nm were measured using a scanning mobility particle sizer (SMPS; DMA 3081; TSI Inc.) at a time resolution of 7 min in Summer. Equivalent black carbon (eBC) levels were monitored with an aethalometer (AE33, Magee Scientific) at a 1-minute resolution. Ammonia (NH₃) concentrations were measured via cavity ring-down spectroscopy (G2103, Picarro Inc.). The gas was sampled via a Teflon tube (4 mm i.d.; 3.1s residence time). Ozone (O₃) and nitrogen dioxide (NO₂) concentrations were tracked using the O₃41M and AS32M gas analyzers (both from Environment S.A.), respectively. Meteorological parameters such as



195

196

197 198

199

200

201 202

203

204 205

206

207208

209

210

211



temperature, relative humidity, wind speed and direction, global radiation, and precipitation were recorded with a compact weather sensor (WS700, Lufft) installed on the container roof. Additional meteorological data was measured by the Institute of Meteorology of the LMU on top of the institute at about 30 m above ground level (https://www.meteo.physik.uni-muenchen.de/request-beta/). The vertical aerosol distribution was assessed using a scanning aerosol Lidar (Rametrics Inc., Type: LR111-ESS-D200, named KASCAL. Fiber laser-induced fluorescence (FILIF) detects formaldehyde (HCHO) by exciting molecules at 353 nm and measuring fluorescence above 370 nm. The technique alternates between on-peak and off-peak laser frequencies to determine HCHO concentration with high specificity. Calibrated against FTIR standards, FILIF achieves ± 27 pptv precision (10-15% accuracy) at 10 Hz sampling frequency, unaffected by humidity. All the information could be found in previous studies (Ye et al., 2021). Unless otherwise specified, all measured values are reported as mean ± standard deviation. Please note that this work is linked to the recently established low-cost sensor network in downtown Munich, monitoring especially O₃, NO₂ and PM_{2.5} (Chen, 2025). This included frequent comparison measurements between reference instruments on a bicycle platform, the instruments in our container, a LfU regulatory monitoring station, and the low-cost sensor network in downtown Munich. Back trajectories were calculated using the Hybrid Single-Particle Lagrangian Integrated Trajectory (HYSPLIT) model (Stein et al., 2015) at 500 m altitude with 72-hour backward duration to identify potential source regions and transport pathways influencing air quality at the measurement site.

2.2.4 PMF analysis

212 The PMF receptor model is a bilinear algorithm that separates air pollutant time series into sources characterized by factor profiles, time series, and residuals (Paatero and Tapper, 1994; Paatero, 1999). It is widely used to identify 213 particle and VOC sources (Kim et al., 2004; Reyes-Villegas et al., 2016; Huang et al., 2018; Gkatzelis et al., 2021). 214 215 PMF has also been applied to inorganic aerosol components, elemental composition of particulate matter (PM), VOC, PAHs, black carbon, and size-resolved particle data, showing its versatility as a receptor model across 216 various pollutant types (Äijälä et al., 2019). PMF has been used for analyzing high-time-resolution elemental data 217 in PM2.5 and PM10 to identify urban and industrial sources and to separate fine and coarse particle sources 218 219 (Reizer et al., 2021). Reviews and guidelines from European air quality agencies explicitly mention the use of PMF applied to particle mass, ions, metals, and gaseous species (like VOC and PAHs) in addition to OA for 220 comprehensive source apportionment studies (Belis et al., 2013). In summary, PMF receptor modeling is broadly 221 222 used and suitable for source apportionment of multi-pollutant data sets. To investigate the sources of VOC, SVOA, and OA, we conducted PMF analysis on VOC mass spectra from 223 PTR-MS, semi-volatile aerosol species measured by CHARON-PTR-MS, and OA measured by HR-TOF-AMS, 224 respectively. The PMF analysis in this study incorporated both VOC and SVOA as distinct input matrices. For 225 226 VOC-PMF, inputs were derived from PTR-TOF-MS data following the methodology of Song et al. (2024), involving comprehensive preprocessing including mass spectral deconvolution, background subtraction, and error 227 matrix calculation where uncertainties were determined as $[(0.1 \times \text{concentration})^2 + (0.5 \times \text{LOD})^2]^{1/2}$ (Kajos et al., 228 2015). SVOA-PMF inputs were obtained through two complementary measurement modes: HEPA-filtered air 229 230 samples (representing background signals) and direct atmospheric sampling (Dir) capturing real-time conditions, with ions (primarily $C_xH_y^+$, $C_xH_yO_z^+$, and $C_xH_yO_zN_n^+$). Both datasets underwent rigorous quality control 231 procedures. Low-molecular-weight species (m/z \leq 60) were excluded to eliminate potential interferences from 232





fragments and common atmospheric gases that may not be representative of specific emission sources (Zhang et al., 2011). Additionally, compounds with ≥20% missing data points were removed to ensure statistical robustness in the PMF analysis, following established protocols for PMF data preparation (Ulbrich et al., 2009; Zhang et al., 2011). The analyses were initially processed using SoFi Pro 9.0 (Datalystica Ltd.) for exploratory factor analysis and data visualization. The source apportionment of organic aerosols (m/z 12-120) was then conducted through unconstrained AMS-PMF analysis using the PMF Evaluation Tool (v3.08C) within IGOR Pro (v8.04), which maintains legacy algorithms specifically optimized for AMS datasets, particularly for handling nonlinear m/z signal-uncertainty relationships in typical AMS operating conditions.

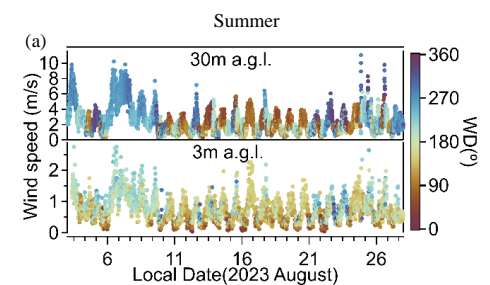
3. Results and discussion

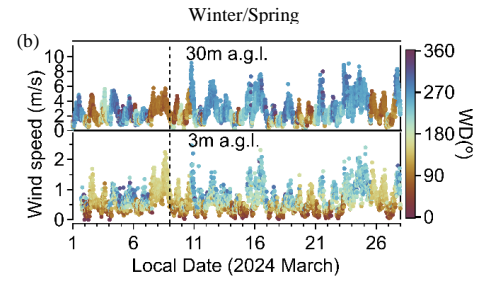
In the first section, we give an overview of the meteorological conditions during the two measurement campaigns and the main characteristics of the observed evolution of aerosol particles and trace gases. The second section will discuss the major sources of aerosol particles and trace gases. In the third section, we focus on strong biomass burning events.

3.1 Overview of observations during summer and wintertime

3.1.1 Overview of meteorological and particle observations

The summer period was characterized by frequent sunny weather with moderate to high temperatures and significant precipitation events mainly at the beginning and end of the summer campaign. The late winter/spring period shows typical winter conditions until March 8th, according to temperature, precipitation followed by more spring-like conditions thereafter.







253

254

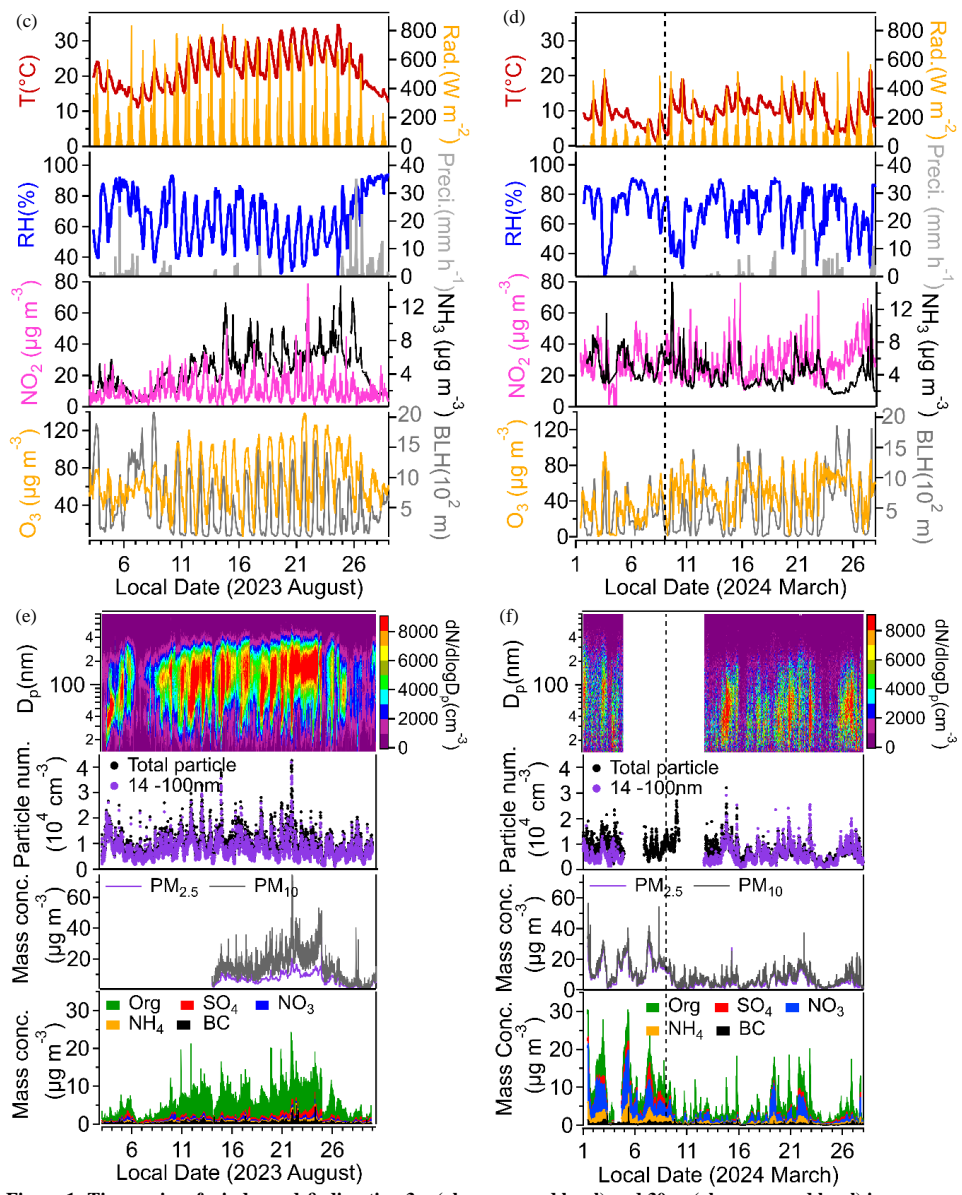


Figure 1: Time series of wind speed & direction 3m (above ground level) and 30 m (above ground level) in summer (a) and winter (b); temperature (T); global radiation (Ra); relative humidity (RH); precipitation; NO₂; NH₃; O₃ and boundary layer height (BLH*) in summer (c) and winter (d); Particle number size distributions; particle number of total and below 100nm ultrafine particles; $PM_{2.5}$ and PM_{10} mass concentrations; Organic aerosol (OA), sulfate, nitrate, and ammonium; Equivalent black Carbon (eBC) in summer (e) and (f) in winter; #All data plotted except the wind data were measured at the container roof. *Please note that the BLH data refer to ERA5 reanalysis data (Guo et al., 2024).

Wind measurements at 3 m and 30 m above ground (Figure 1a-b) revealed consistent vertical gradients across all seasons, with average speeds of 0.7 ± 0.4 and 2.6 ± 1.4 m s⁻¹, respectively. Meteorological conditions varied significantly between seasons (Figure 1c-d), creating distinct chemical environments. The higher summer





temperatures (21.9 ± 5.8 °C) promoted enhanced biogenic emissions and photochemical activity, while lower winter temperatures (8.4 ± 3.0 °C) favored primary pollutant accumulation. Relative humidity and total precipitation showed minimal seasonal variation. NO₂ concentrations were 2.5-2.8 times higher in winter/spring $(26.1 \pm 9.9 / 28.4 \pm 10.8 \,\mu g \,m^{-3})$ than summer $(10.2 \pm 7.7 \,\mu g \,m^{-3})$ due to increased heating emissions and reduced photolysis under shallow boundary layers (339 \pm 298 m /510 \pm 477 m vs 516 \pm 453 m, variability). The LfU station showed similar winter $(27.2 \pm 9.2 \,\mu g \, m^{-3})$ and early spring $(27.8 \pm 9.2 \,\mu g \, m^{-3})$ mean concentrations to Theresienstrasse, but exhibited weak temporal correlation, reflecting the strong spatial variability of NO₂. Notably, summer NO₂ at LfU (23.4 \pm 10.1 μ g m⁻³) was 2.3 times higher than Theresienstrasse, yet temporal correlation improved substantially (R = 0.5) in Figure S5. This seasonal pattern suggests that summer's higher boundary layer enhanced vertical mixing and local photochemical reactions, increasing spatial differences in mean NO2 levels. However, stronger synchronized daily photochemical cycles improved temporal agreement between the two sites. Gaseous NH₃ showed elevated concentrations across all seasons, with winter $(5.4 \pm 1.5 \,\mu g \, m^{-3})$ and spring $(4.0 \pm 1.5 \,\mu g \, m^{-3})$ 1.8 µg m⁻³) levels comparable to summer values (4.8 ± 2.6 µg m⁻³). O₃ concentrations at Theresienstrasse exhibited strong seasonal variation, with highest levels in summer (67.1 \pm 26.6 μg m⁻³), followed by early spring (52.2 \pm 19.3 $\mu g m^{-3}$), and lowest in late winter (32.4 \pm 20.2 $\mu g m^{-3}$). The LfU station showed similar seasonal patterns (summer: $59.3 \pm 25.5 \,\mu g \, m^{-3}$; late winter: $30.8 \pm 17.3 \,\mu g \, m^{-3}$; early spring: $45.9 \pm 17.2 \,\mu g \, m^{-3}$) with strong temporal correlations (R = 0.8 in August 2023; R = 0.7 in March 2024) in Figure S5, indicating consistent O₃ behavior across both sites driven by regional photochemical processes.

Particle size distributions revealed contrasting seasonal patterns driven by different formation mechanisms (Figures 1e-f). Summer showed the highest total particle number concentrations ($10000 \pm 5100 \text{ cm}^{-3}$) with a substantial variability dominated by ultrafine particles (< 100 nm: $80.6 \pm 8.2\%$), indicating enhanced new particle formation under intense photochemical conditions and elevated precursor concentrations. Winter exhibited lower total number concentrations ($8900 \pm 3500 \text{ cm}^{-3}$) but a lower fraction of ultrafine particles ($33.6 \pm 10.1\%$), consistent with reduced photochemical activity and primary emission dominance. Spring showed intermediate behavior with high ultrafine fractions (89.7%) but lower absolute number concentrations. The seasonal PM mass concentrations showed opposite trends to the particle number concentrations: winter PM_{2.5} peaked at $13.0 \pm 7.4 \text{ µg m}^{-3}$ with nitrate as the dominant component due to low temperatures, shallow boundary layers and increased residential heating. In contrast, summer ($6.7 \pm 3.7 \text{ µg m}^{-3}$) and spring ($4.2 \pm 3.1 \text{ µg m}^{-3}$) showed lower PM_{2.5} levels dominated by organic aerosols, despite higher particle numbers, suggesting predominance of freshly formed ultrafine particles that contribute little to total mass.

Aerosol particle mass composition varies significantly by season, reflecting different formation mechanisms. Organic aerosol particles dominate in summer due to high photochemical activity (Figures 2), averaging $4.3 \pm 2.9 \, \mu g \, m^{-3}$, higher than $3.3 \pm 1.7 \, \mu g \, m^{-3}$ in winter and $1.8 \pm 1.8 \, \mu g \, m^{-3}$ in spring. Nitrate is the main component in winter $(4.5 \pm 3.2 \, \mu g \, m^{-3})$ due to low temperatures favoring particle phase and increased heating emissions providing abundant NH₃ and NO_x precursors for ammonium nitrate formation. Nitrate concentrations drop significantly in spring $(1.0 \pm 1.3 \, \mu g \, m^{-3})$ and summer $(0.3 \pm 0.2 \, \mu g \, m^{-3})$ as rising temperatures shift the equilibrium toward the gas phase. Ammonium follows similar patterns, peaking in winter $(1.8 \pm 1.1 \, \mu g \, m^{-3})$ and remaining low in warmer seasons (spring: $0.4 \pm 0.4 \, \mu g \, m^{-3}$; summer: $0.3 \pm 0.2 \, \mu g \, m^{-3}$), consistent with reduced ammonium nitrate formation.





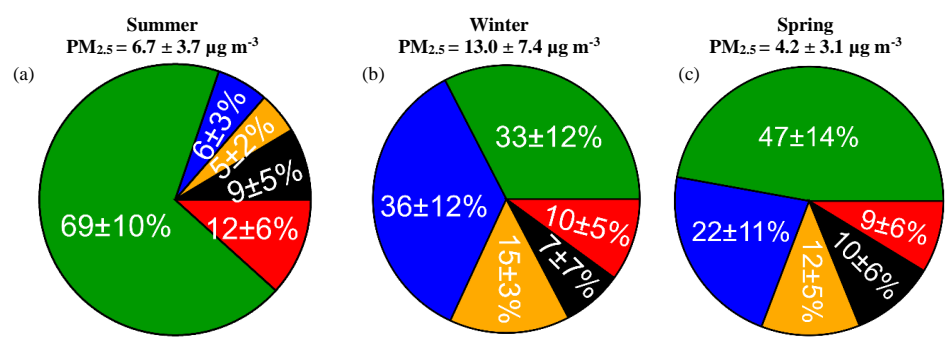


Figure 2: Average fractions of $PM_{2.5}$: OA (green), sulfate (red), nitrate (blue), ammonium (yellow) and eBC (black) in summer (a), (b) in winter (until March 8^{th}) and (c) in spring based on AMS and Aethalometer measurements.

3.1.2 Diurnal behaviour of gaseous BVOC and BTEX

The average diurnal variations of key volatile organic compounds (VOC) are examined below, focusing on major biogenic and anthropogenic species, including BTEX—a group of aromatic hydrocarbons comprising benzene, toluene, ethylbenzene, and xylene. The VOC selected here comprise $32.3 \pm 13.1\%$ of all VOC detected in summer, $41.0 \pm 12.9\%$ in winter and $37.9 \pm 12.5\%$ in spring.

Figure 3 illustrates the diurnal variations of six VOC across three seasons, revealing distinct patterns tied to their sources and environmental influences. Isoprene and monoterpenes, both biogenic VOC, exhibit the highest mixing ratios in summer. However, Isoprene displays a bimodal pattern in summer and spring, with concentration peaks

ratios in summer. However, Isoprene displays a bimodal pattern in summer and spring, with concentration peaks during the morning and evening hours, suggesting a potential link to traffic activity during the morning and evening hours. This is consistent with direct measurements of isoprene in vehicle exhaust by Borbon et al. (2001). Additionally, fragmentation of higher-carbon aldehydes and cycloalkanes from anthropogenic sources may contribute to the signal of isoprene, further complicating source attribution in urban environments (Coggon et al., 2024). Monoterpene exhibited early morning peaks in summer and spring, but was almost flat in winter. In contrast, their concentrations are minimal in winter due to suppressed biological activity. Anthropogenic VOC like benzene, toluene, xylene, and trimethylbenzene show different seasonal behaviors. Benzene peaks in winter, likely due to lower BLH and reduced dispersion, with dips at midday possibly from increased OH radical oxidation under sunlight. Toluene, xylene, and trimethylbenzene display notable spikes in spring, particularly during morning and evening hours, suggesting strong contributions from traffic emissions and industrial activities.



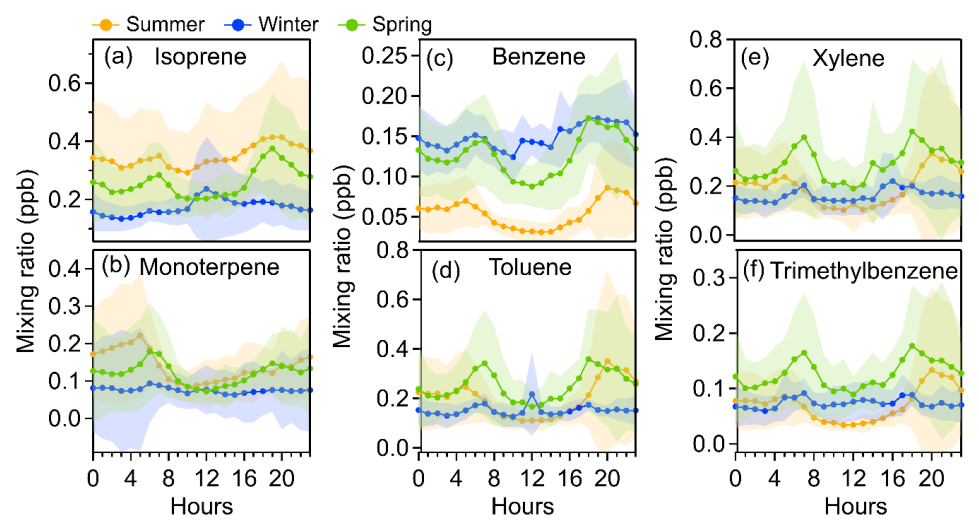


Figure 3: Diurnal behavior of (a) Isoprene, (b) Monoterpenes, (c) Benzene, (d) Toluene, (e) Xylene and (f) Trimethylbenzene in summer, winter and spring.

3.2 Sources of VOC and organic aerosol particles

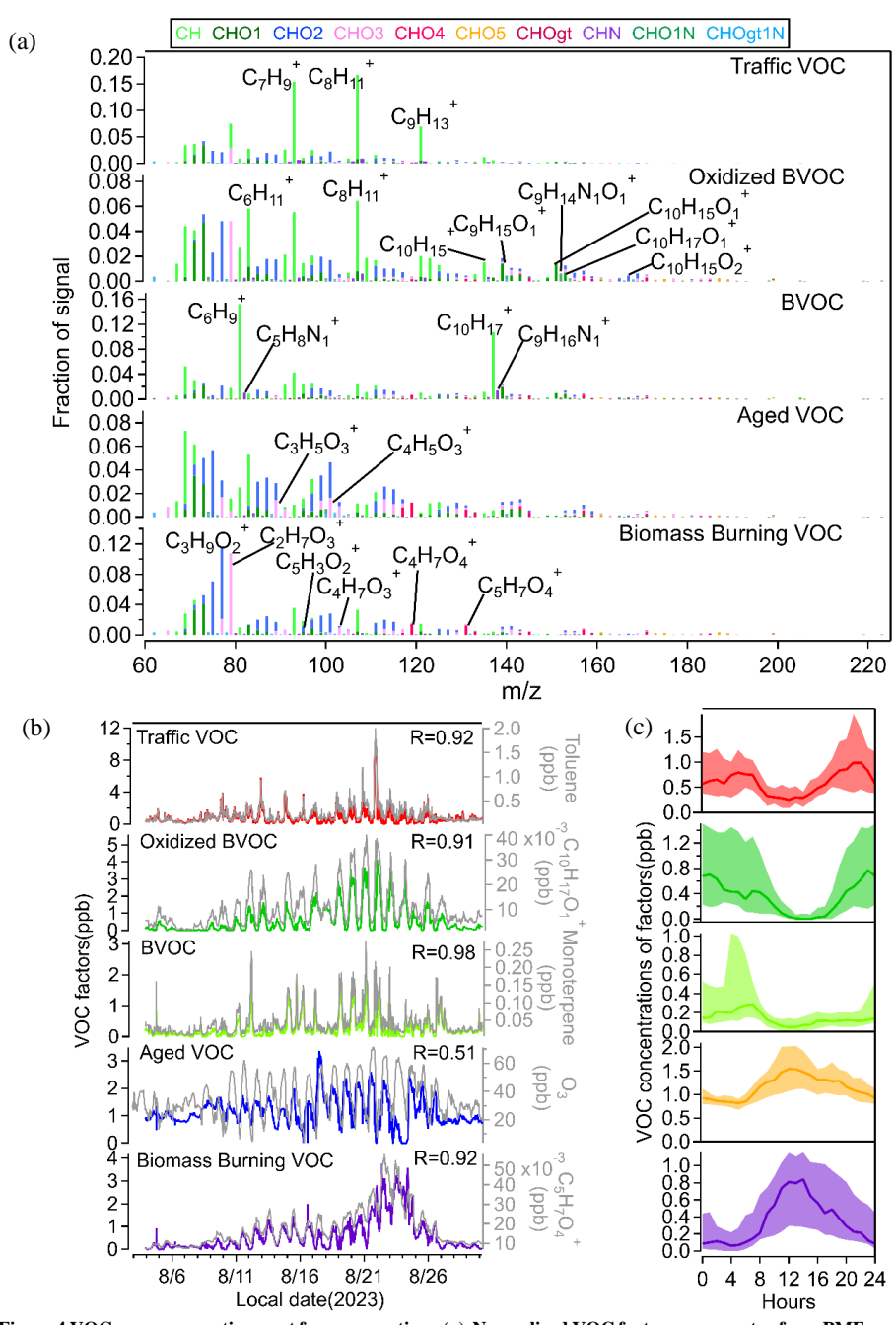
In this section we use statistical (PMF) analysis of on-line mass spectra from VOC (PTR-MS) and semi-volatile organic aerosol particles (CHARON-PTR-MS) as well as organic aerosol particles (HR-TOF-AMS) to determine their major sources.

3.2.1 VOC sources in summer and winter

We included 117 VOC ions (Table S2) for PMF analysis in summer and 97 VOC ions (Table S3) in winter/spring, excluding abundant ions that could skew results and very low ion signals with minimal impact. Abundant ions (e.g., fragments of alkanes or oxygenated VOC) were removed because their high concentrations may lead to over-representation of certain factors, while low-signal ions were excluded to reduce noise interference (Song et al., 2024). The average VOC molecules mixing ratio is 3.4 ± 1.0 ppb in summer, 2.1 ± 0.7 ppb in winter, and 3.4 ± 1.7 ppb in spring. This study thoroughly examined factor profiles, diurnal patterns, and correlations with tracers (Figure 4, S6 and Table S4) for summer and for winter (Figures S7, S8 and Table S5). Five factors were identified based on measured VOC as the optimal interpretable solutions for summer and winter, respectively.







Figure~4~VOC~source~apportionment~for~summer~time.~(a)~Normalized~VOC~factor~mass~spectra~from~PMF~analysis~and~characteristic~mass~peaks~in~summer;~(b)~Time~series~of~VOC~factors~including~traffic,~oxidized~BVOC,~BVOC,~aged~VOC,~and~biomass~burning~VOC;~(c)~Median~diurnal~variations~in~VOC~factors~during~summer~time

326





In summer, the first factor was characterized by high contributions and strong correlations with aromatic 327 hydrocarbon ions, such as $C_7H_9^+$ (m/z 93.07), $C_8H_{11}^+$ (m/z 107.086), and $C_9H_{13}^+$ (m/z 121.102). These compounds 328 correspond to toluene, xylenes, and C₉-aromatics, commonly used as vehicular emission markers (Squires et al., 329 2020; Jain et al., 2022). We assigned it to traffic VOC. These ions show a correlation coefficient (R) of 330 331 approximately 0.9 with traffic emissions (Table S3). According to the diurnal profiles of traffic (Figure 4) in summer, it shows distinct peaks during morning and evening hours. 332 The second factor was classified as weakly oxidized BVOC. It was identified by oxidation products of 333 monoterpenes, specifically $C_9H_{15}O_1^+$ myrcenol (m/z 139.112), $C_{10}H_{13}O_1^+$ carvone (m/z 149.097), weakly-oxidized 334 335 molecules of monoterpenes $C_{10}H_{15}O_1^+$ (m/z 151.112), $C_{10}H_{17}O_1^+$ (m/z 153.128) and $C_{10}H_{15}O_2^+$ (m/z 167.107) (Li et al., 2020a). These ions show strong correlations with the Oxidized BVOC factor, with R values of 0.93, 0.93, 336 0.93, 0.91, and 0.87, respectively. Oxidized BVOC have a nighttime peak in the diurnal profile and drop to nearly 337 338 zero by noon, likely due to enhanced dilution and quicker oxidation to oxidation states not detectable by PTR-339 The third factor was identified as BVOC due to the predominance of $C_{10}H_{17}^+$ monoterpene (m/z 137.133) and its 340 341 fragmentation C₆H₉⁺ (m/z 81.07) ions in this VOC factor, with correlations of 0.98 and 0.86, respectively. 342 Sesquiterpenes also show a strong correlation with this factor (R=0.80). The average diurnal behavior of BVOC shows an early morning peak, because BVOC, especially monoterpenes, are often stored in vegetation and 343 344 released at the start of the morning due to sunlight and slight temperature increases (Malik et al., 2023), combined 345 with a shallow boundary layer that keeps emissions near the surface. The fourth factor showed a good correlation with butyric acid $C_3H_5O_3^+$ (m/z 89.024) and $C_4H_5O_3^+$ (m/z 101.024), 346 with R values of 0.75 and 0.72, respectively. The time series of O₃ and this factor showed a good correlation 347 348 during certain periods. The diurnal cycle of it exhibits a daytime peak, indicating involvement in photochemical 349 oxidation processes. We classified it as aged VOC. 350 The fifth factor, biomass burning VOC, is dominated by propylene glycol C₃H₉O₂⁺ (m/z 77.06) and orthoacetic acid C₂H₇O₃+ (m/z 79.039), with strong correlations of 0.85 and 0.83, respectively. Additionally, a ring fragment 351 352 of oxidized syringol, C₄H₇O₄+ (m/z 119.034), and ring fragments of oxidized guaiacol and syringol molecules $C_5H_3O_2^+$ (m/z 95.013), $C_5H_7O_4^+$ (m/z 131.034) and $C_4H_7O_3^+$ (m/z 103.04) contribute smaller fractions but display 353 even higher correlations, with values of 0.90, 0.91, 0.92 and 0.86 (Yee et al., 2013). Compared with the other 4 354 factors, the biomass burning VOC mass spectrum has more oxidized compounds. 355 356 In late winter and early spring, the first factor was identified as traffic VOC using the same method as in summer, showing high contributions and strong correlations with aromatic hydrocarbon ions, including toluene C₇H₉+ (m/z 357 93.07), C_9 aromatics $C_9H_{13}^+$ (m/z 121.102), and cymene $C_{10}H_{13}^+$ (m/z 133.102) in Figures S7, S8 and Table S5. 358 359 The second factor, classified as terpenes VOC, was marked by the predominance of monoterpene $C_{10}H_{17}^{+}$ (m/z 137.133) and its fragment C₆H₉⁺ (m/z 81.07) ions with correlations of 0.90 and 0.89, respectively. Sesquiterpenes 360 also show a strong correlation (R=0.92). The diurnal variation shows both morning and evening peaks, with the 361 morning peak being higher than the evening peak. This pattern differs from typical traffic trends. This pattern is 362 363 similar to that of limonene from shower gels (Yeoman et al., 2020), which shows higher concentrations in the morning compared to the evening. It correlates with the traffic factor because people typically shower in the 364 morning before leaving home, leading to higher detection. By the evening, the limonene has dissipated. 365

https://doi.org/10.5194/egusphere-2025-5191 Preprint. Discussion started: 20 November 2025 © Author(s) 2025. CC BY 4.0 License.





The biomass burning VOC factor included a lot of smaller oxygenated VOC (OVOC) such as 1,3-propanediol 366 $C_3H_9O_2^+$ (m/z 77.06), acetic anhydride $C_4H_7O_3^+$ (m/z 103.04), 2-furoic acid $C_5H_5O_3^+$ (m/z 113.024), maleic acid 367 C₄H₅O₄+ (m/z 117.019), butanedioic acid C₄H₇O₄+ (m/z 119.034), benzoic acid C₇H₇O₂+ (m/z 123.045) (Lemieux 368 et al., 2004) and salicylic acid $C_7H_7O_3^+$ (m/z 139.04). They all show strong correlations (R=0.85-0.90) with this 369 370 factor. Notably, C₅H₅O₃⁺ and C₇H₇O₃⁺ are recognized as tracers of biomass burning VOC (Li et al., 2020b; Romanias et al., 2024). It displays a peak during the daytime, possibly due to biomass burning activities in certain 371 areas (e.g., cooking or outdoor grilling), which increase VOC emissions and lead to a daytime peak in the VOC 372 diurnal profile. 373 374 The fourth factor was dominated by xylene, represented by C_8 -aromatic hydrocarbon $C_8H_{11}^+$ (m/z 107.086), with a correlation of 0.96. This factor also shows a strong correlation with 3-ethyl-pyridine C₇H₁₀N₁⁺ (m/z 108.081) 375 and the C₉-aromatic hydrocarbon VOC C₉H₁₃⁺ (m/z 121.102), with correlations of 0.98 and 0.91, respectively. 376 377 Xylene and trimethylbenzene are components of flue gases from fossil fuel combustion VOC (Niu et al., 2021). It also displays morning and evening peaks in its diurnal cycle, leading to its identification as a traffic VOC. 378 The fifth factor has minimal correlation with most masses, only showing a correlation of 0.73 with benzene (C₆H₇⁺) 379 380 and weak correlations with various oxygenated compounds. Therefore, this factor may originate from different 381 low-concentration emission sources. Its diurnal variation shows a small evening peak, likely influenced by traffic or industrial emissions. This factor accounts for $54\% \pm 9\%$ in late winter, decreasing to $23\% \pm 16\%$ in early spring 382 due to the increased temperature (Figure 5), and as background VOC are commonly found to have a high 383 384 proportion, we classify it as background VOC. The source contributions of VOC vary significantly across seasons, reflecting shifts in emission patterns and 385 atmospheric conditions. In summer, the largest contributor is aged VOC at 42 ± 18%, indicating the dominance 386 of secondary pollutants formed through atmospheric photochemical oxidation processing. Traffic emissions 387 388 account for 22 ± 14%, while oxidized biogenic VOC make up 13 ± 13%, and fresh BVOC contribute 7 ± 7%. 389 Biomass burning plays a notable role at $16 \pm 15\%$, likely due to outdoor barbeque in warmer months. Winter exhibits a different profile, with background sources dominating at 54 ± 9%, suggesting stable atmospheric 390 391 conditions. Traffic-related emissions split into two categories—traffic1 ($26 \pm 6\%$) and traffic2 ($7 \pm 6\%$)—possibly reflecting different vehicle types or fuel usage patterns. Monoterpenes VOC remain low $(4 \pm 4\%)$, consistent with 392 reduced biogenic activity and from anthropogenic source like personal care products (Wu et al., 2024), while 393 biomass burning contributes $8 \pm 6\%$, potentially from residential heating. In spring, the contributions are traffic1 394 395 $22 \pm 7\%$, monoterpene VOC increased to $9 \pm 9\%$ as vegetation becomes more active, biomass burning VOC $33 \pm 9\%$ 14%, traffic2 13 \pm 8%, and background 23 \pm 16% (Figure 5). 396



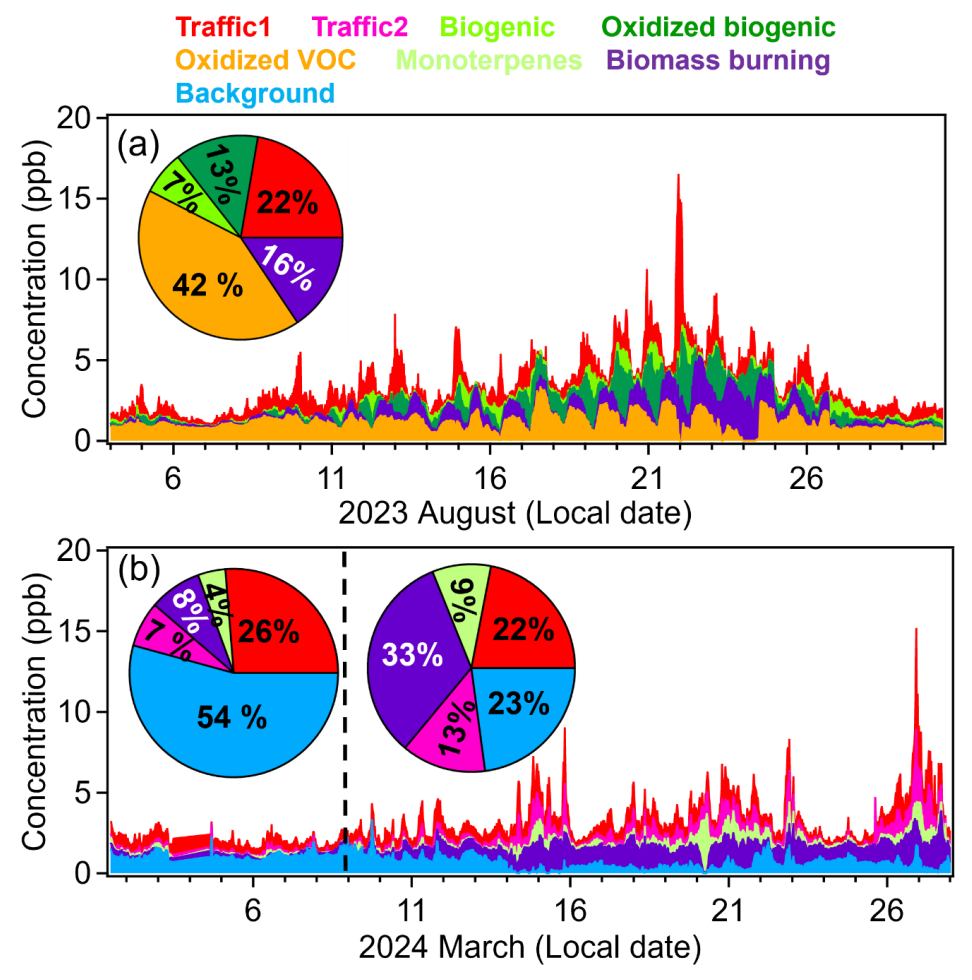


Figure 5: The time series and relative mass contribution (pie charts) of each VOC factor to total VOC concentrations in summer (a), winter (left of the dash line) and spring (right of the dash line) (b).

3.2.2 Sources of semi-volatile organic aerosol (SVOA)

We included 153 SVOA ions (Table S6) for PMF analysis for summer and 171 VOC ions (Table S7) for winter/spring, excluding abundant ions that could skew results and very low ion signals with minimal impact (Song et al., 2024). The average semi-volatile organic aerosol concentration was $0.3 \pm 0.2 \,\mu g \, m^{-3}$ in summer, 0.14 \pm 0.08 $\,\mu g \, m^{-3}$ in winter and 0.07 \pm 0.07 $\,\mu g \, m^{-3}$ in spring. Through a comprehensive analysis of factor profiles, diurnal variations, and tracer correlations in summer (Figure S9, S10, and Table S8) and in winter (Figure S11, S12, and Table S9). Five semi-volatile organic aerosol (SVOA) factors were identified as the best interpretable solution for different seasons. In summer, the first factor showed distinct signals from primary oxidation products of terpenes, including oxidized monoterpenes $C_{10}H_{15}O_1^+$ (R=0.93) and $C_{10}H_{17}O_1^+$ (R=0.89) (Li et al., 2020a). While the expected monoterpene





408 oxidation products are typically $C_9H_{15}O_{1-5}^+$, we found that $C_9H_{13}O_{1}^+$ and $C_9H_{13}O_{2}^+$ also correlated well with this factor, with correlation coefficients R=0.91 and R=0.85, respectively. This suggests that the C₉H₁₅O_{1.2}+ 409 compounds may lose hydrogen, forming C₉H₁₃O₁⁺ and C₉H₁₃O₂⁺ (Gkatzelis et al., 2018b). Additionally, nitrogen-410 containing species like C₉H₁₃N₁O₁, C₉H₁₂N₁O₂, and C₉H₁₃N₁O₅ displayed high intensity and significant 411 412 correlation with this factor, which may indicate they are fragments of monoterpene-derived organic nitrates, such as C₉H₁₅N₁O₅₋₇ (Massoli et al., 2018). The diurnal cycle shows a nighttime peak (Figure S10c), which we have 413 attributed this factor to weakly oxidized biogenic organic aerosol (Weakly OBOA) based on the presence of a 414 monoterpene oxidation tracer and the observed diurnal pattern. 415 416 The second factor includes clear markers of isoprene oxidation products, specifically C₅H₈O_n species (Li et al., 2020a), with $C_5H_9O_6^+$ (R=0.83) and $C_5H_9O_3^+$ (R=0.82) showing strong correlations (Riva et al., 2016). 417 Additionally, the ion with the highest fraction, C₃H₅O₄⁺ (R=0.85), likely originates from the oxidation of 418 419 ISOPOOH (Rios, 2018). However, benzoic acid C₇H₇O₂⁺ (R=0.95), showing a strong signal, and phthalic anhydride C₈H₅O₃⁺ (R=0.83) are both known emissions from biomass burning aerosols (Bruns et al., 2017; Koss 420 et al., 2018). $C_6H_8O_5$ (R=0.84) (Molteni et al., 2018) is an oxidation product of benzene, while $C_7H_{10}O_6$ (R=0.84) 421 422 as reported by Nakao et al. (Nakao et al., 2011), is an oxidation product of o-cresol, an emission from oxygenated 423 aromatic BBOA. Therefore, we define this factor as mixed oxidized isoprene OA and BBOA. The third factor was identified as BBOA due to its strong correlation (R=0.88) with vanillic acid C₈H₈O₄ (Fleming 424 425 et al., 2020) and its prominent fragment (C₈H₆O₄) with even higher correlation (R=0.96), which constitutes a 426 significant portion of this factor. Additionally, another BBOA tracer, syringic acid (C₉H₁₀O₅) (Wan et al., 2019), and its fragment (C₉H₆O₃, R=0.95), likely formed by the loss of two H₂O molecules, or as a direct BBOA emission 427 (Fleming et al., 2020), further support this identification. Other ions, such as $C_6H_6O_5$ and $C_7H_8O_5$, are oxidation 428 products of guaiacol (Yee et al., 2013). The diurnal cycle of this factor, peaking during the daytime, suggests that 429 430 barbecue events may be contributing sources during the summer. 431 The fourth factor shows no correlation with other compounds and exhibits a distinct nighttime peak (Figure S10c). However, it correlates strongly with nitrate detected by AMS (R = 0.71). This suggests that the factor represents 432 433 regional background, with its nighttime increase likely influenced by local accumulation effects. 434 The fifth factor was identified as more oxidized monoterpene OA, comprising highly oxidized monoterpene products such as $C_{10}H_{15}O_{3.5}^+$ (R=0.86, 0.85, 0.84), diacetin $C_7H_{13}O_{5}^+$ (R=0.79), oxidized molecules of 435 436 monoterpenes $C_8H_{13}O_2^+$ (R=0.81), $C_8H_{13}O_4^+$ (R=0.80), and its fragment ($C_8H_{11}O_3^+$, R=0.83). Compounds like 437 C₉H₁₃O₃₋₄ (R=0.81, 0.78) likely arise from fragments of the C₉H₁₄O_n series, representing more oxidized monoterpene products that have lost hydrogen. Compared to the diurnal pattern of less oxidized terpene products, 438 this factor's peak displays a delay, suggesting that primary oxidation products form initially and then undergo 439 440 further oxidation, resulting in more oxidized BOA (More OBOA). In winter and spring, the first factor is identified as night-time aged BBOA due to the presence of distinct BBOA 441 tracers, $C_6H_6N_1O_4^+$ and $C_7H_8N_1O_4^+$ (Figure S12a), which do not appear in the mass spectra of other factors. 442 Nitrocatechols (C₆H₅N₁O₄) originates from anthropogenic activities, including biomass burning and vehicle 443 444 emissions. Meanwhile, methyl-nitrocatechols (C₇H₇N₁O₄) are specific markers for BBOA, as they are formed from m-cresol released during biomass combustion and diesel exhaust (Kourtchev et al., 2016). These tracers also 445 exhibit the same strong correlation of 0.97 with this factor (Table S8). Syringic acid (C9H10O5) also correlates 446 447 well (R=0.70) with this factor. In terms of its daily cycle did not show peaks during morning or evening rush





448 hours; instead, a peak was observed around 8 p.m., suggesting it aligns more with BBOA. This factor showed a 449 strong correlation with highly oxidized nitrogen-containing compounds and secondary organic aerosols (syringic acid). This factor is more related to highly oxidized nitrogen-containing secondary organic aerosols, indicating 450 that nitrogen-containing compounds produced by BBOA may have undergone significant oxidation by NO3 451 452 radicals. Therefore, I identified it as night-time aged BBOA. The second factor was characterized by a high fraction of oleic acid C₁₈H₃₅O₂⁺ (R=0.90), C₁₆H₃₅O₃⁺ 453 $(C_{16}H_{33}O_2(H_2O)^+)$ (R=0.88), $C_{16}H_{33}O_2^+$ corresponding to palmitic acid (R=0.54), and $C_{16}H_{31}O_1^+$ is the fragment 454 of C₁₆H₃₃O₂+ (R=0.54). C₁₈H₃₄O₂ is identified as the cooking tracer oleic acid, while C₁₆H₃₃O₂+ serves as another 455 456 cooking aerosol tracer, corresponding to palmitic acid (Reyes-Villegas et al., 2018; Wang et al., 2020b; Huang et al., 2021). $C_{16}H_{31}O_1^+$ is thought to originate from $C_{16}H_{33}O_2^+$ due to fragmentation involving the loss of one H_2O 457 molecule. These findings strongly suggest that this factor represents cooking aerosol. 458 459 The third factor was identified as aged combustion. In this factor, the aromatic hydrocarbon C₇H₉⁺ accounts for a relatively higher fraction and exhibits a strong correlation (R = 0.79). Although C₈H₁₃⁺ does not contribute 460 significantly as C₇H₉⁺, it also shows the same strong correlation. These compounds are attributed to combustion 461 sources (Wang et al., 2022). The ion $C_7H_{10}N_1^+$, potentially a fragment of acridine $(C_7H_{12}N_1^+)$ originating from 462 463 coal combustion (Wang et al., 2021), exhibits a distinct signal and the highest correlation (R = 0.94). Similarly, $C_6H_{15}O_3^+$ (R = 0.93) corresponds to 2-methoxyethyl ether (MXEE), a product of fuel combustion. Monoterpene 464 oxidation products, such as $C_{10}H_{17}O_1^+$ (R = 0.86) and $C_9H_{13}O_1^+$ (R=0.82), are also observed. This is likely because 465 466 monoterpenes, serving as biofuel components in engines and boilers, form oxidized monoterpene products when combusted and oxidized (Philippe Dagaut et al., 2024). Additionally, benzocaine C₉H₁₂N₁O₂+ exhibits strong 467 correlation (R = 0.80) with this factor and is likely a product of oxidized combustion processes. 468 The fourth factor has C_6 carboxylic acids $(C_6H_7O_5^+)$ which is the phenol oxidation products with OH radicals in 469 470 the low-NO_x system, and $C_7H_9O_5^+$ denoted as the guaiacol with OH adduct. Propanedioic acid $(C_3H_5O_4^+)$, 471 pentanedione (C₄H₅O₃⁺), and 2-oxopentanedioic acid C₅H₇O₄⁺ are fragments derived from the OH oxidation products of biomass burning VOC (BBVOC) such as guaiacol and syringol (Yee et al., 2013). Additionally, 472 473 C₆H₆O₂ is an OH radical oxidation product from phenol. A higher fraction of 2,5-di-(hydroxymethyl)furan 474 C₆H₉O₃⁺ was observed, which may result from C₆H₇O₂⁺ binding with a water molecule. These photochemical products, formed from BBVOC oxidation by OH radicals, confirm that this factor represents aged BBOA. All the 475 476 aforementioned ions exhibit a strong correlation of approximately 0.85 with this factor, as shown in Table S2. 477 Furthermore, its diurnal pattern, with a peak at 15:00 during the day, leads to its identification as day-time aged BBOA. 478 The fifth factor shows a very strong correlation with stearic acid $C_{18}H_{37}O_2^+$ (R = 0.95), $C_{16}H_{33}O_2(H_2O)^+$ (R = 0.91), 479 480 $C_{18}H_{15}O_{1}^{+}$ (R = 0.90), $C_{19}H_{15}O_{1}^{+}$ (R = 0.88), and oleic acid $C_{18}H_{35}O_{2}^{+}$ (R = 0.88). However, these compounds do not account for significant fractions in this factor's mass spectrum as they do in factor 2's mass spectrum. Notably, 481 trimethoxy methane C₄H₁₁O₃⁺ is a key ion in this factor but contributes minimally to others and shows no 482 correlation with the factor (R = 0.02). While the composition includes unrelated compounds, its strong correlation 483 484 with sulfate detected by AMS (R=0.74) suggests a regional background origin, with the nighttime peak indicating local accumulation effects. 485 During summer, the composition of SVOA includes $11 \pm 15\%$ weakly OBOA, $16 \pm 15\%$ oxidized isoprene & 486

BBOA (mixture of oxidized isoprene OA and BBOA), 25 ± 21% BBOA, 30 ± 22% attributed to regional





background sources, and $18\pm16\%$ to More OBOA (Figure 6). In winter, nighttime aged BBOA accounts for $10\pm9\%$, cooking OA contributes $4\pm5\%$, aged combustion OA makes up $9\pm10\%$, daytime aged BBOA constitutes the largest fraction at $55\pm21\%$, and regional background sources contribute $23\pm17\%$. In spring, nighttime aged BBOA accounts for $12\pm12\%$, cooking OA contributes $11\pm12\%$, aged combustion OA makes up $24\pm18\%$, daytime aged BBOA constitutes the largest fraction at $46\pm25\%$, and regional background sources contribute $7\pm9\%$.

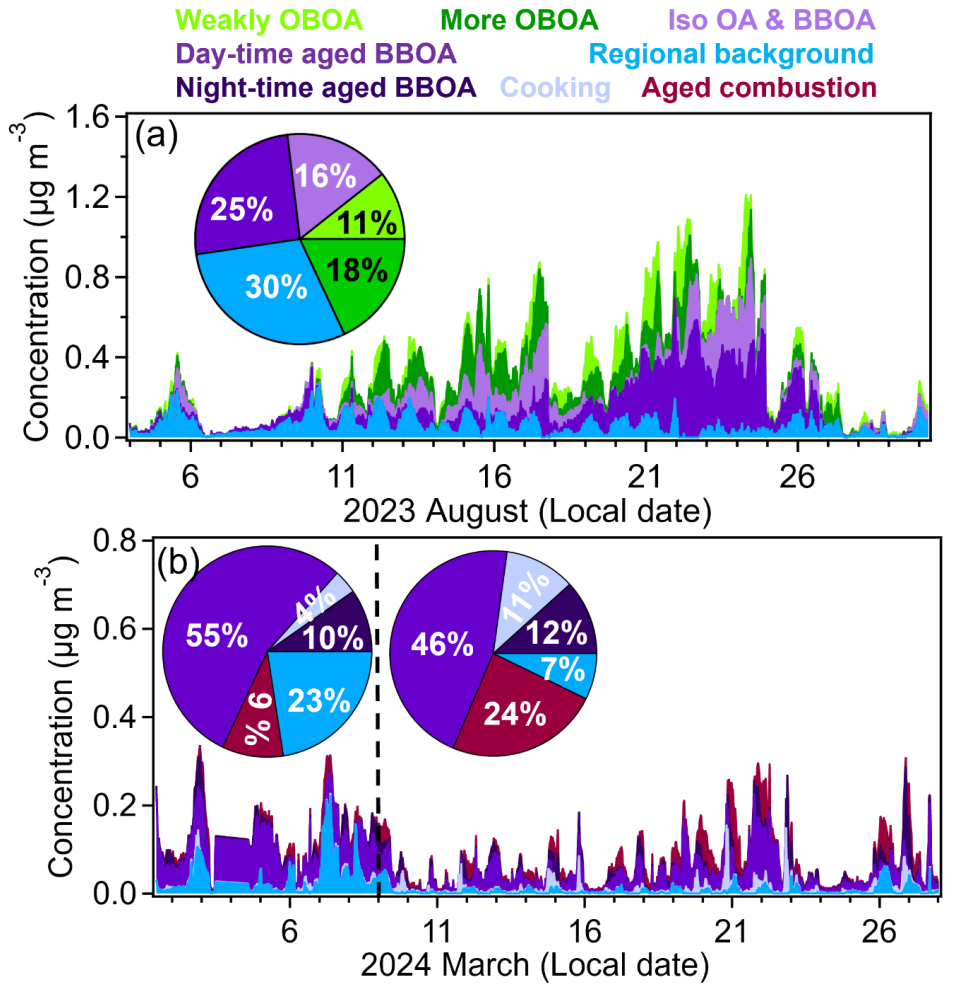


Figure 6: The time series and relative mass contributions (pie charts) of each SVOA factor to total SVOA concentrations in summer (a), winter (left of the dash line), and spring (right of the dash line) (b).

3.2.3 Sources of organic aerosol particles

This study thoroughly examined source factor profiles, diurnal patterns, and correlations with tracers (FigureS13, S14, S15, S16 and S17) for OA particles. The average organic aerosol concentration was $4.3 \pm 2.9 \,\mu g \, m^{-3}$ in





summer, $3.4 \pm 1.7 \,\mu g \, m^3$ in winter and $1.8 \pm 1.8 \,\mu g \, m^3$ in spring. Five OA factors were identified as the optimal 498 interpretable solutions for summer and winter/spring, respectively. 499 In summer, the first factor was identified as cooking organic aerosol (COA), based on its high H: C ratio (1.82), 500 low O: C ratio (0.19) (Figure S14a), higher contributions at m/z 55 (C₃H₃O⁺) and m/z 57 (C₃H₅O⁺), and the mass 501 502 spectrum dominated by hydrocarbon ions. These characteristics are consistent with reported COA in urban areas (Elser et al., 2016; Äijälä et al., 2017; Liu et al., 2018). Additionally, fatty acid (C₁₆H₃₅O₃⁺) detected by 503 CHARON-PTR showed a moderate correlation (R = 0.54) with the COA time series (Figure 14b). The second 504 factor is characterized by a mass spectrum also dominated by hydrocarbon ions, a similar O: C ratio, and a high 505 506 O: C ratio, but with higher contributions at m/z 55 ($C_4H_7^+$) and m/z 57 ($C_4H_9^+$) (Elser et al., 2016). These features are consistent with the characteristics of hydrocarbon-like organic aerosol (HOA) which is related to traffic. 507 additionally, HOA shows a good correlation (R= 0.66) with the eBC time series. The third factor is assigned to 508 509 Biogenic secondary organic aerosol (BOA), based on its H: C ratio of 1.63 and O: C of 0.44. The O/C ratio falls within the range typically associated with semi-volatile oxidized organic aerosol (SVOOA), which is 510 approximately 0.35 ± 0.14 (Setyan et al., 2012). And it has a good correlation of 0.86 with monoterpene oxidation 511 products (pinonaldehyde) in CHARON-PTR. BOA's diurnal pattern (Figure S14c) shows an increase starting at 512 8 pm, reaching its peak at 7 am. This trend aligns with the nighttime oxidation process of monoterpenes, 513 supporting its identification as BOA. The fourth factor was identified as aged biomass burning organic aerosol 514 515 (BBOA) because its O/C ratio of 0.597 is slightly higher than that of fresh BBOA (0.15-0.5) and falls within the range of aged BBOA (0.5-0.87) (Ortega et al., 2013). Its diurnal shows a small peak at 3 pm and a higher peak at 516 10 pm, the nighttime peak indicates that fresh BBOA happened rapid dark aging process (Kodros et al., 2020). 517 And it shows a strong correlation (R=0.93) with BBOA tracer levoglucosan detected by CHARON-PTR. therefore, 518 the fourth factor is identified as aged BBOA. The fifth factor has the lowest H: C ratio (1.43) and the highest O:C 519 ratio 0.75, which falls within the range of low-volatility oxygenated organic aerosol (LVOOA) (0.6-1.0) (J. L. 520 521 Jimenez et al., 2009). LVOOA is dominated by CO⁺ and CO₂⁺ and shows a strong correlation (R=0.70) with O₃, 522 indicating that it is associated with photochemical oxidation processes (Kumar et al., 2016). Its diurnal pattern shows a daytime peak. These characteristics align well with the typical properties of LVOOA, leading to its 523 identification as LVOOA. To ensure that every tracer detected by CHARON-PTR and correlated with AMS-PMF 524 factors is representative, we compared different related fatty acids, toluene and trimethyl benzene, different 525 monoterpene oxidation products, and different BBOA tracers. All of them showed good time-series correlations 526 527 (Figure S16). 528 In winter, we identified all the factors using the same method as in summer. The difference is that the traffic diurnal cycle (Figure S15e) exhibits distinct peaks during the morning and evening rush hours. Fresh BBOA 529 shows an evening peak, indicating evening residual heating activities. Aged BBOA is characterized by its 530 correlation with C₆H₇O₅⁺, which we identified as an oxidation product of BBOA in the CHARON-PTR section. 531 its diurnal pattern is very flat, suggesting it may be associated with regional background levels or long-range 532 533 transport. for LVOOA, NH₄⁺ is used as an indicator, as it correlates strongly with inorganic aerosol during autumn and winter (Freney et al., 2011). Other different OA factors time series shown in Figure S17. 534 535 In summer, OA contributions are as follows: traffic 8 ± 8%, cooking 11 ± 13%, BOA 22 ± 14%, aged BBOA 25 \pm 21%, and LVOOA 33 \pm 20%. In winter, the contributions are: traffic 5 \pm 4%, cooking 12 \pm 12%, fresh BBOA 536





 $13 \pm 9\%$, aged BBOA $36 \pm 12\%$, and LVOOA $33 \pm 17\%$. In spring, the contributions are: traffic $9 \pm 7\%$, cooking $19 \pm 16\%$, fresh BBOA $27 \pm 17\%$, aged BBOA $37 \pm 19\%$, and LVOOA $9 \pm 10\%$ (Figure 7).

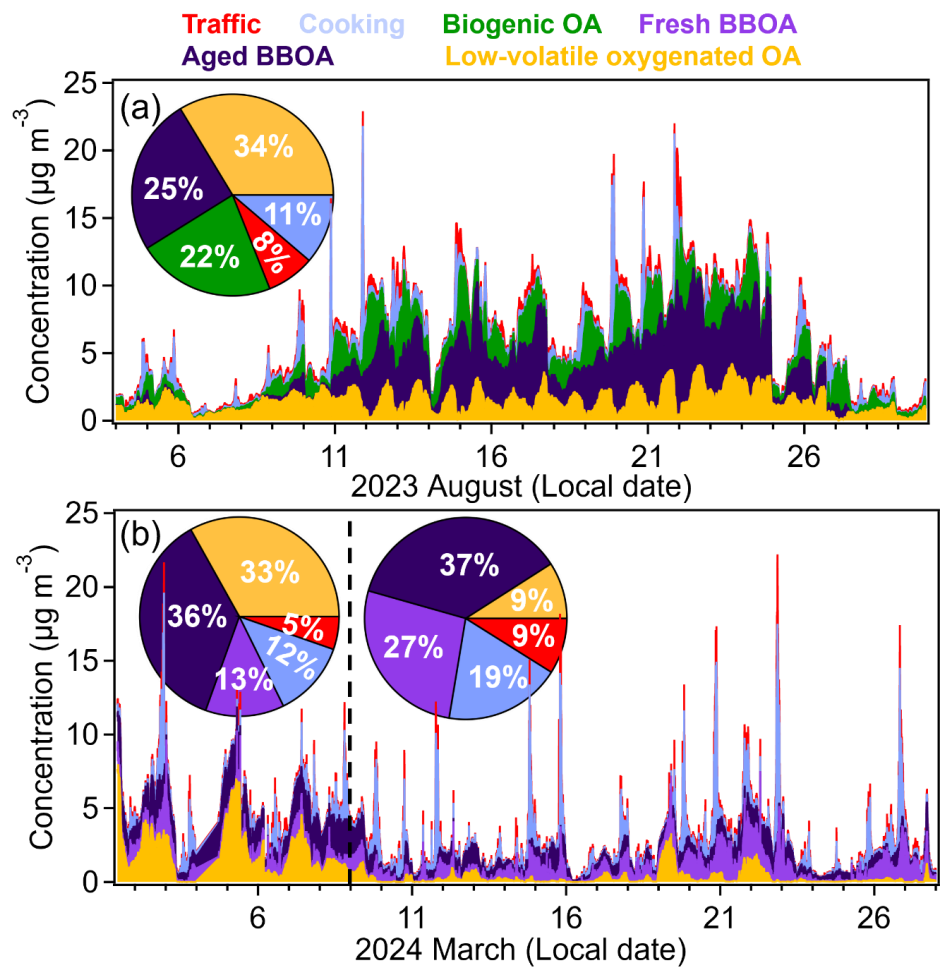


Figure 7: The time series and relative mass contributions (pie charts) of each OA factor to total OA concentrations in summer (a), winter (left of the dash line), and spring (right of the dash line) (b).

Previous PMF studies in Stuttgart and Karlsruhe identified consistent summer source patterns: traffic-related OA contributes less than 10%, SV-OOA accounts for approximately 16%, while LV-OOA dominates at around 75% of OA mass. This LV-OOA prevalence indicates strong biogenic influence from regional vegetation and photochemical processes enhanced by higher summer temperatures. In Stuttgart, elevated winter PM_{2.5} stems primarily from biomass burning and residential heating, evidenced by enhanced levoglucosan and nitrated phenol signals, alongside increased traffic-related primary OA (POA). Both traffic OA and BBOA contribute substantially, though LV-OOA remains significant. Karlsruhe experiences similar source patterns with increased residential heating, traffic emissions, and coal combustion from industrial sources, but benefits from less severe inversion and stagnation conditions, resulting in lower overall concentrations. Munich's intermediate winter





 pollution levels suggest a source composition transitioning between these profiles, warranting detailed PMF analysis to characterize its specific emission contributions and compare with the established patterns in Stuttgart and Karlsruhe.

PMF source apportionment reveals strong seasonal dependencies in organic aerosol composition, with summer conditions driving the majority of aerosol burden in Munich. Summer demonstrates the highest concentrations across all source categories, dominated by aged BBOA ($2.3~\mu g~m^{-3}$) as the largest single contributor due to barbeque charcoal combustion. Photochemical LV-OOA ($1.5~\mu g~m^{-3}$) and biogenic emissions ($1.4~\mu g~m^{-3}$) emerge exclusively during summer, reflecting enhanced secondary aerosol formation under high temperatures and intense solar radiation that promote both biogenic emissions and photochemical processing. In contrast, late winter and spring show dramatically reduced organic aerosol levels, with late winter contributions limited primarily to regional background ($0.4~\mu g~m^{-3}$) and minimal aged BBOA ($0.4~\mu g~m^{-3}$). Traffic and cooking emissions remain consistently minor throughout all seasons ($\leq 0.7~\mu g~m^{-3}$), suggesting these local primary sources are less significant compared to secondary formation processes and regional biomass burning influences.

SVOA and OA composition exhibits distinct seasonal patterns driven by varying source emissions and atmospheric processing. Summer periods show elevated OA concentrations due to enhanced photochemical oxidation under high solar radiation, promoting secondary organic aerosol formation (Figure 8). Biogenic sources contribute significantly during summer through increased vegetation emissions. Rapid atmospheric oxidation transforms fresh BBOA to aged BBOA, explaining the predominance of aged BBOA despite active barbecue activities. In late winter, residential heating dominated fresh BBOA emissions. During early spring, both heating and barbecue emissions contributed to fresh BBOA, with the latter increasing as temperatures rose. Consequently, Fresh BBOA concentrations increased from late winter to early spring. However, Fresh BBOA became less detectable in peak summer due to accelerated aging processes under higher temperatures and enhanced photochemical activity. Late winter and spring show substantial aged BBOA from residential heating activities. Cooking and traffic emissions remain consistent year-round sources, though their oxidation efficiency increases significantly in summer compared to winter and early spring when photochemical processes are less active.

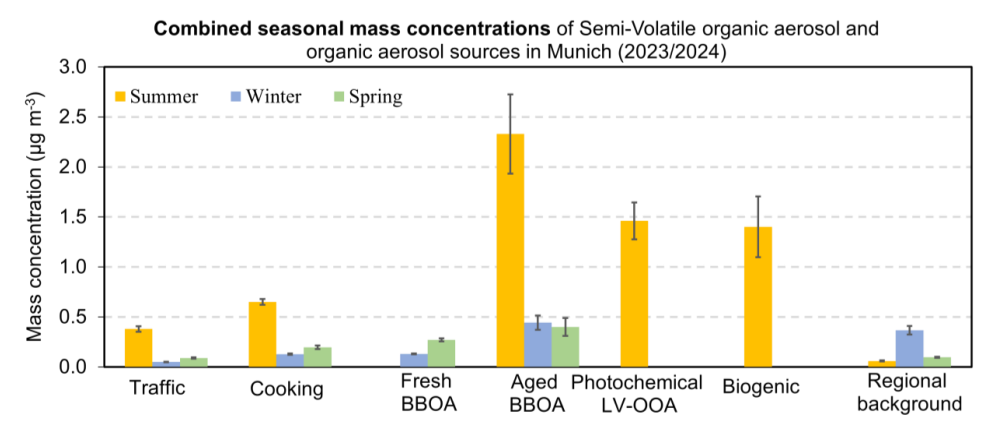


Figure 8: Comprehensive seasonal mass contributions of SVOA and OA sources in Munich summer, winter and spring time (Source categories combine factors from Charon-PTR-MS and HR-TOF-AMS: Aged BBOA (day-time aged BBOA, night-time aged BBOA, and IsoOA & BBOA from Charon; aged BBOA from AMS), Biogenic OA (weakly OBOA and More OBOA from Charon; BOA from AMS), with remaining sources combined similarly). Please note,



585

586

587

588

589 590

591

592

593

594

595

596

597

598

599

600

601

602

603

604

605

606 607

608

609 610

611

612

613

614

615

616 617



that the total OA concentrations were $4.3 \pm 2.9 \, \mu g \, m^{-3}$ in summer, $3.4 \pm 1.7 \, \mu g \, m^{-3}$ in winter, and $1.8 \pm 1.8 \, \mu g \, m^{-3}$ in spring.

3.3 Seasonal strong biomass burning aerosol events

PMF analysis of AMS mass spectra reveals that aged BBOA substantially contributes to total OA with seasonal variations: $25 \pm 21\%$ in summer, $36 \pm 12\%$ in winter, and $37 \pm 19\%$ in spring. Two prominent BBOA events were observed during August $22^{\text{nd}} - 24^{\text{th}}$ (OA: $7.9 \pm 1.7 \, \mu \text{g m}^{-3}$) and March $7^{\text{th}} - 9^{\text{th}}$ (OA: $3.3 \pm 1.3 \, \mu \text{g m}^{-3}$).

During August 2023, aged BBOA showed strong correlations with multiple biomass burning indicators (Figure 9 and Table S10). The high correlation with eBC (R=0.75) suggests significant light-absorbing carbon from combustion processes. Primary biomass burning tracers showed excellent correlations: levoglucosan (C₆H₁₁O₅+, R=0.93) and syringic acid (C₉H₁₁O₅⁺, R=0.84), confirming fresh biomass burning emissions. The strong correlation with atmospheric oxidation products such as C₆H₇O₅⁺ (R=0.88, phenol oxidation products from OH radical reactions under low-NO_x conditions) and C₇H₉O₅⁺ (R=0.87, guaiacol-OH oxidation products) indicates significant photochemical aging processes during summer. Notably, aged BBOA correlated strongly with barbecue charcoal combustion tracers including formaldehyde (R=0.80) (Kabir et al., 2010), coniferyl alcohol $(C_{10}H_{13}O_3^+, R=0.90)$, pinic acid $(C_9H_{15}O_4^+, R=0.76)$, and homovanilic acid $(C_9H_{11}O_4^+, R=0.83)$ (Vicente et al., 2018). These consistently high correlations (R > 0.75) strongly suggest that the aged BBOA factor during summer months is predominantly attributed to barbecue activities, as these compounds are characteristic markers of charcoal and wood combustion used in outdoor cooking rather than other biomass burning sources. However, during the intensive BBOA episode (August 22nd-24th), most tracer correlations decreased slightly, and formaldehyde showed no correlation with aged BBOA (R= -0.20) in Table S10. This suggests that during highconcentration events, different source contributions alter the chemical fingerprint, possibly indicating the influence of additional fresh emissions or changes in atmospheric processing conditions. Back trajectory analysis during the strong BBOA event shows that 51% of air masses originated from long-range transport near the Belgium border (average BBOA: 5.3 µg m⁻³), while 15% from the Bavarian region exhibited the highest concentrations (7.3 µg m⁻³) in Figure S18. Given the absence of wildfire sources and the strong correlations with barbeque charcoal combustion tracers, we attribute the elevated concentrations primarily to outdoor barbeque charcoal combustion emissions.

In the whole March 2024, aged BBOA exhibited markedly different correlation patterns, indicating distinct sources and processes. The weaker correlation with eBC (R=0.39) suggests different combustion characteristics compared to summer. Most importantly, aged BBOA showed poor correlations with barbecue charcoal combustion tracers: formaldehyde (R=0.14), coniferyl alcohol (R=0.47), pinic acid (R=0.41), and homovanilic acid (R=0.51). The dramatic decrease in these correlations compared to summer values indicate minimal contribution from outdoor cooking activities during winter months. Primary biomass burning markers also showed reduced correlations: levoglucosan (R=0.30), and syringic acid ($C_9H_{11}O_5^+$, R=0.24), suggesting different emission sources or processing pathways. Conversely, aged BBOA maintained strong correlations with guaiacol oxidation products: $C_6H_7O_5^+$ (R=0.80) and $C_7H_9O_5^+$ (R=0.74). This pattern strongly indicates that winter aged BBOA primarily originates from residential heating emissions that have undergone atmospheric oxidation (Kodros et al., 2020). The guaiacol derivatives are characteristic markers of wood combustion for heating purposes, and their predominant correlations with aged BBOA confirm this source attribution. In contrast, fresh BBOA showed strong

https://doi.org/10.5194/egusphere-2025-5191 Preprint. Discussion started: 20 November 2025 © Author(s) 2025. CC BY 4.0 License.



625

626

627 628

629 630

631

632

633

634 635

636 637

638 639

640

641

642

643 644

645

646 647



correlations with barbecue charcoal combustion tracers: coniferyl alcohol (R=0.69), pinic acid (R=0.68), and homovanilic acid (R=0.67), as well as primary biomass burning markers including levoglucosan (R=0.72) and syringic acid (R=0.62). Notably, fresh BBOA showed weak correlation with the aged oxidation products ($C_6H_7O_5^+$ and $C_7H_9O_5^+$) that strongly correlated with aged BBOA. This divergent correlation pattern suggests that fresh BBOA emitted from residential heating or barbecue charcoal combustion during late winter and early spring undergoes slower atmospheric aging compared to summer conditions, resulting in a clear separation between fresh and aged BBOA characteristics.

The intensive episode analysis (March 7th-9th, 2024) revealed correlation patterns consistent with the monthly analysis (Table S10), reinforcing the conclusion that seasonal BBOA sources shift from barbecue charcoal combustions in summer to residential heating in winter. During this episode, aged BBOA maintained strong correlations exclusively with guaiacol oxidation products (C₆H₇O₅⁺ and C₇H₉O₅⁺), consistent with the monthly pattern. However, fresh BBOA exhibited notably selective correlations, showing moderate relationships only with coniferyl alcohol (R=0.65) and levoglucosan (R=0.62), while displaying weak or negligible correlations with other tracers. The limited correlation pattern of fresh BBOA can be attributed to its substantially lower concentration compared to aged BBOA during this period (Table S10). When aged BBOA dominates the total BBOA mass, the temporal variability of most tracers is primarily governed by the aged component, effectively masking the correlation signals from fresh BBOA. As a minor constituent, fresh BBOA's true relationships with various tracers become statistically obscured, making it challenging to establish robust correlations beyond the most characteristic primary emission markers (i.e., levoglucosan and coniferyl alcohol). This phenomenon highlights the importance of aged BBOA as the dominant source during winter heating periods, while fresh emissions represent localized, transient contributions that are rapidly diluted within the regional aged aerosol background. Back trajectory analysis reveals distinctly different transport patterns compared to summer. Winter air masses predominantly followed three clusters: Cluster 1 (32%) transported through Czechia with BBOA concentrations of 2.3 µg m⁻³, Cluster 2 (14%) originating from Poland passing through Czechia (1.8 µg m⁻³), and Cluster 3 (19%) from the Belarus-Poland border passing through Czechia and Austria (1.1 µg m⁻³) in Figure S18. The dominance of Czechia-influenced trajectories (65%) contrasts sharply with summer patterns, indicating significant contributions from Central European residential heating emissions. The prevalence of aged BBOA in these air masses suggests substantial accumulation of Aged BBOA during long-range transport. Notably, Cluster 2 exhibited elevated fresh BBOA concentrations, evidenced by lower O:C ratios, indicating recent biomass burning emissions from residential heating activities along the Polish transport pathway.



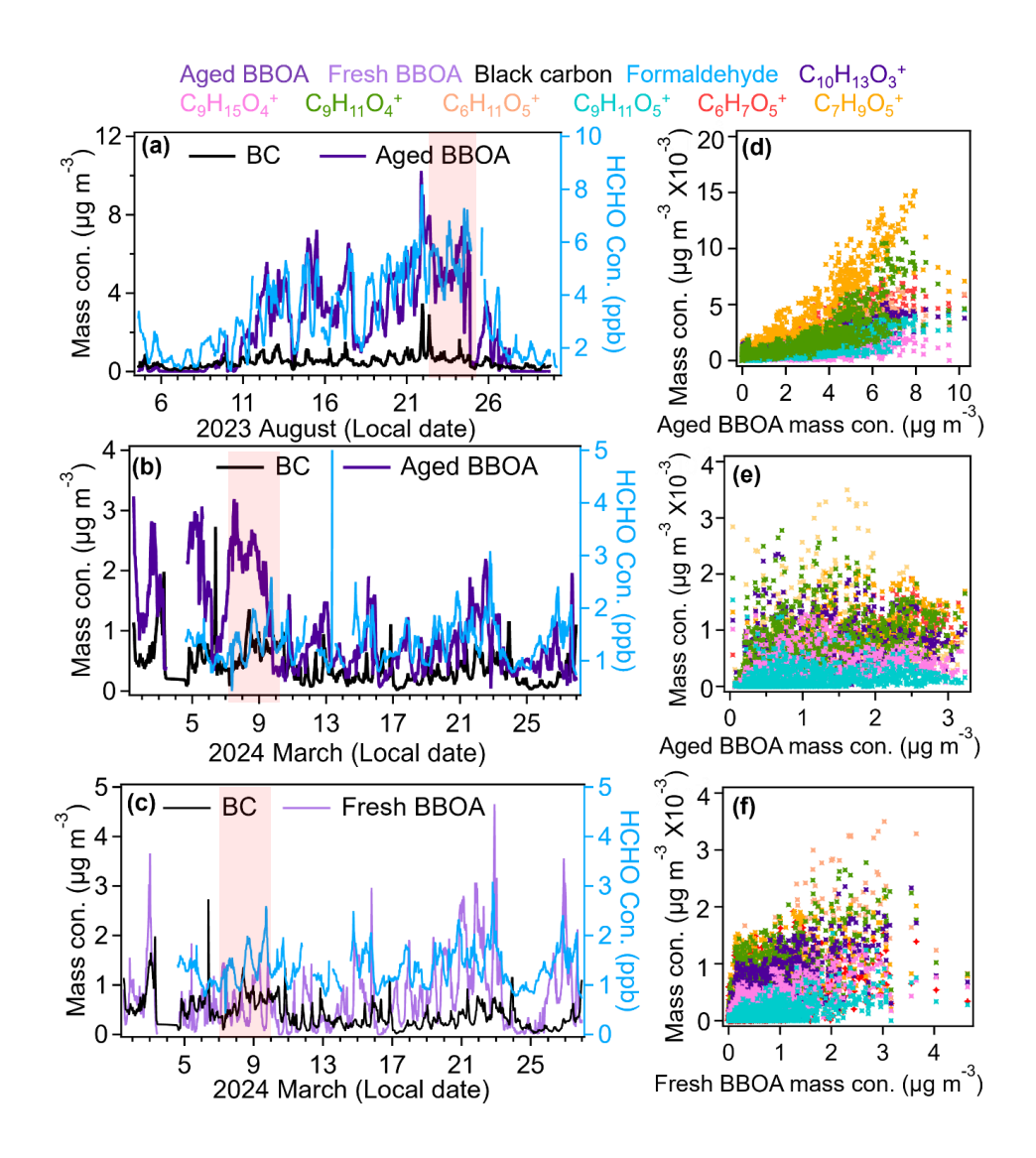


Figure 9. Time series of aged BBOA, black carbon, and formaldehyde during summer (August 2023, a) and winter/spring (March 2024, b) periods and fresh BBOA during March 2024 (c); Scatter plots showing correlations between aged BBOA and barbecue charcoal combustion tracers $(C_{10}H_{13}O_3^+, C_9H_{15}O_4^+, C_9H_{11}O_4^+)$, and biomass burning tracers $(C_6H_{11}O_5^+, C_9H_{11}O_5^+, C_9H_{7}O_5^+, C_9H_{7}O_5^+, C_7H_9O_5^+)$ in summer (d), in winter (e) and Fresh BBOA correlated with all the tracers (f). Strong BBOA events are in red shade.

4. Conclusions

648

649

650

651

652

653

This study investigates the sources, concentrations, and seasonal variations of VOC, SVOA, and OA in an urban street canyon of the third largest German city, Munich, using a combination of online mass spectrometric observations and PMF based source apportionment. The results reveal a complex interplay between anthropogenic and biogenic sources, as well as atmospheric photochemical aging that governs the composition and evolution of the atmospheric pollutants in the urban street canyon.





The PM_{2.5} analysis reveals Munich's distinctive air quality profile for different seasons. During summer, Munich's 654 $PM_{2.5}$ concentrations (6.7 \pm 3.7 μg m⁻³) are comparable to neighboring German cities like Stuttgart (7.1 \pm 3.3 μg 655 m^{-3}) and Karlsruhe (7.0 \pm 3.5 μ g m^{-3}), also reflecting similar regional background conditions. Winter shows greater 656 divergence: Munich's $PM_{2.5}$ levels (13.0 \pm 7.4 μg m⁻³) exceed Karlsruhe's (5.6 \pm 4.9 μg m⁻³) but remain 657 658 substantially lower than Stuttgart's pollution $(27.0 \pm 11.9 \,\mu g \,m^3)$ also caused by stronger industrial sources in a basin like topography (Huang et al., 2019). This intermediate profile becomes even more significant when 659 considering Munich's status as Germany's third-largest city, with a dense urban population and strong economic 660 activity generating complex emission patterns, however, with less classical emissions from heavy industry. 661 662 Compared to other European cities - Paris with winter PM_{2.5} maxima of 15 µg m⁻³, Berlin's with winter frequent PM_{2.5} episodes above 15 µg m⁻³ (the World Health Organization (2021) recommended daily limit), or Bern's 663 winter PM_{2.5} of 14 µg m⁻³ average (Bressi et al., 2013; Grange et al., 2021; Renard et al., 2024) - Munich represents 664 665 a critical test case with high population density, thriving industries and tourism. Our findings identify and quantify a pronounced seasonal regime shift in organic aerosol composition. While a 666 substantial anthropogenic baseline from traffic is persistent, the system transitions from a winter regime 667 dominated by primary biomass burning aerosols (BBOA contributing up to 64% of OA) to a summer regime 668 669 governed by photochemical aging (LVOOA at 33%) and formation of secondary biogenic aerosol. Critically, we demonstrate that biomass burning is not confined to the heating season. The significant and rising contribution 670 from barbecue emissions in spring and summer reveals an underappreciated, health-sensitive emission source 671 672 (Lenssen et al., 2022; Xu et al., 2023; Gruber and Kalamas, 2024). The seasonal evolution of BBOA provides critical insights into its atmospheric processing. The presence of both 673 fresh and aged BBOA in winter (fresh: $13 \pm 9\%$; aged: $36 \pm 12\%$) and spring (fresh: $27 \pm 17\%$; aged: $37 \pm 19\%$) 674 contrasts sharply with the aerosol composition in summer, where only aged BBOA ($25 \pm 21\%$) is detected. This 675 676 pattern strongly indicates that primary biomass burning emissions undergo rapid atmospheric oxidation in summer, with substantial conversion to the aged type driven by enhanced photochemical activity (e.g., higher temperatures, 677 radiation, and O3 levels). This rapid aging process for BBOA (Kodros et al., 2020; Li et al., 2023) presents a 678 679 marked contrast to the typically slower, multi-generational oxidation pathway of anthropogenic VOCs from traffic 680 (Srivastava et al., 2022), which require substantial atmospheric processing to form condensable SOA. A key implication of this finding is that if biomass burning OA persists in the atmosphere despite rapid aging processes, 681 then mitigation strategies targeting primary biomass burning emissions could yield more immediate air quality 682 683 benefits. We identified nocturnal oxidation of biogenic VOC as a significant SOA formation pathway in summer. The substantial contribution of biogenic VOCs (oxidized BVOC: $13 \pm 13\%$, and BVOC: $7 \pm 7\%$), coupled with 684 BOA from oxidized monoterpenes ($22 \pm 14\%$), demonstrates that nocturnal oxidation (primarily by O_3 and NO_3 685 radicals) generates secondary aerosol yields comparable those from daytime photochemical production (e.g., 686 LVOOA at $33 \pm 20\%$). Consequently, monoterpene emission profiles must be treated as a critical air quality 687 parameter and considered in urban vegetation management (Ren et al., 2014). It should be taken into account that 688 the urban green can have positive but also negative impact on the pollution levels of aerosol particles. 689 690 Previous studies in Stuttgart and Karlsruhe (Huang et al., 2019; Song et al., 2022; Zhang et al., 2024) identified traffic-related OA contributions consistently at or below 10% during summer. Munich exhibits similar patterns, 691 with traffic OA contributing $8 \pm 8\%$ in summer, $5 \pm 4\%$ in winter, and $9 \pm 7\%$ in spring. This consistency across 692

all three cities in southwest Germany indicates that traffic is a minor OA component, exhibiting only relatively



695

696

697 698

699

700

701 702

703

704 705

706

707 708

709

710 711

712

713 714

715

716

717

718

721



small seasonal variations. The most significant difference emerges in the abundance of LV-OOA. In Stuttgart and Karlsruhe, LV-OOA dominates summer OA with approximately 75%, reflecting strong biogenic influence from regional vegetation and photochemical processes enhanced by higher temperatures. In contrast, Munich's LV-OOA remains substantially lower and relatively stable for different seasons (33 \pm 20% summer, 33 \pm 17% winter, 9 ± 10% spring), indicating either reduced biogenic precursor emissions or weaker photochemical oxidation despite comparable regional conditions. In Stuttgart, elevated winter PM2.5 stems primarily from biomass burning and residential heating, evidenced by enhanced levoglucosan and nitrated phenol signals. Both traffic OA and BBOA contribute substantially to winter pollution. Karlsruhe exhibits similar patterns, with residential heating, traffic emissions, and coal combustion from industrial sources driving winter PM_{2.5} increases. Munich's source profile diverges markedly from both cities. BBOA contributes substantially more to Munich's OA composition year-round compared to Stuttgart and Karlsruhe. Summer shows notable BBOA contribution (aged BBOA $25 \pm$ 21% combined with BOA $22 \pm 14\%$), and winter BBOA dominance increases dramatically (fresh BBOA $13 \pm 9\%$ plus aged BBOA 36 ± 12%). Spring displays the highest BBOA contribution (fresh BBOA 27 ± 17% plus aged BBOA 37 ± 19%), indicating sustained biomass burning influence extending beyond residential heating into recreational activities. This persistent, elevated BBOA signature distinguishes Munich as a BBOA-dominated system, contrasting with the LV-OOA-dominated profiles of Stuttgart and Karlsruhe, and suggests that biomass burning requires year-round mitigation strategies in Munich. In summary, this work reveals the dynamic chemical evolution of urban aerosol. The interplay between primary emissions from heating and cooking, the relatively constant traffic baseline, and the seasonally-modulated photochemical and nocturnal monoterpene chemistry creates a complex but decipherable pollution phenotype. Future research should prioritize tracking the atmospheric evolution of key source markers (e.g., from barbecues especially in summer and spring) to constrain their aging timescales and health-relevant properties. Integrating these process-level insights is paramount for refining air quality models like PALM-4U (Zhang et al., 2024; Resler et al., 2024; Samad et al., 2024) to accurately predict effectivity of measures to improve air quality in future urban scenarios.

719 **Conflict of interests statement:**

Two co-authors are co-editors of ACP but the authors declare that there is no conflict of interests.

Author contributions

FK, JC, and HS conceived the concept, planned, and organized the campaign. YXL did the AMS and PTR-MS measurements, analyzed most of the data and wrote the manuscript with contributions from all co-authors. HS planned and organized the measurements, took care of the particle number, size and additional trace gas measurements. HZ, SA, AW, JC and FK supported instrument set up and conducted lidar measurements. XS, YWL and FK checked and calibrated the instruments during the measurements. JBS, ZA, and JS contributed to data analysis. TL contributed to planning of the measurement campaign and reviewed the manuscript.





728 Data availability

729 The data used in this study is available at the KIT data repository KITopen data (doi will be added here).

730 Acknowledgement

- 731 We gratefully acknowledge the support by the meteorological department of the Ludwig-Maximilians-University
- 732 of Munich (Group of Prof. Bernhard Mayer) and especially Markus Garhammer. The support by the technical
- 733 team (Group of Steffen Vogt) of the Institute of Meteorology and Climate Research Atmospheric Aerosol
- Research of the Karlsruhe Institute of Technology was extremely helpful.

Funding

735

- 736 The China Scholarship Council (CSC) provided PhD scholarships for Yanxia Li and Xuefeng Shi. The KIT
- 737 Graduate School for Climate and Environment (GRACE) supported Yanxia Li. The KIT funded the campaign in
- 738 the program "Changing Earth Sustaining our Future" of the Helmholtz Association. The campaign was partly
- funded by the Institute for Advanced Study, Technical University of Munich (Grant no. 291763). The TUM
- authors are partly supported by ERC Consolidator Grant CoSense4Climate (Grant 101089203) and Bavarian State
- 741 Ministry of the Environment (Grant TLK 01U-75487).

742 **5. References**

- 743 Äijälä, M., Daellenbach, K. R., Canonaco, F., Heikkinen, L., Junninen, H., Petäjä, T., Kulmala, M., Prévôt, A. S.
- H., and Ehn, M.: Constructing a data-driven receptor model for organic and inorganic aerosol a synthesis
- 745 analysis of eight mass spectrometric data sets from a boreal forest site, Atmos. Chem. Phys., 19, 3645-3672,
- 746 10.5194/acp-19-3645-2019, 2019.
- 747 Äijälä, M., Heikkinen, L., Fröhlich, R., Canonaco, F., Prévôt, A. S. H., Junninen, H., Petäjä, T., Kulmala, M.,
- 748 Worsnop, D., and Ehn, M.: Resolving anthropogenic aerosol pollution types deconvolution and exploratory
- classification of pollution events, Atmospheric Chemistry and Physics, 17, 3165-3197, 10.5194/acp-17-3165-
- 750 2017, 2017.
- 751 Allison C. Aiken, Peter F. DeCarlo, Jesse H. Kroll, Douglas R. Worsnop, J. Alex Huffman, Kenneth S. Docherty,
- 752 Ingrid M. Ulbrich, Claudia Mohr, Joel R. Kimmel, Donna Sueper, Yele Sun, Qi Zhang, Achim Trimborn,
- 753 Megan Northway, Paul J. Ziemann, Manjula R. Canagaratna, Timothy B. Onasch, M. Rami Alfarra, and Prevot,
- 754 A. S. H.: O/C and OM/OC Ratios of Primary, Secondary, and Ambient Organic Aerosols with High-
- 755 Resolution Time-of-Flight Aerosol Mass Spectrometry, Environmental Science & Technology, 42, 4478-4485,
- 756 2008.
- 757 Messwertarchiv LfU Bayern: https://www.lfu.bayern.de/luft/immissionsmessungen/messwertarchiv/index.htm,
- 758 last access: 29.09.
- 759 Belis, C. A., Larsen, B. R., Amato, F., El Haddad, I., Favez, O., Harrison, R. M., Hopke, P. K., Nava, S., Paatero,
- P., Prévôt, A., Quass, U., Vecchi, R., and Viana, M.: European Guide on Air Pollution Source Apportionment
- vith Receptor Models, European Commission, Joint Research Centre, Institute for Environment and
- Sustainability, Luxembourg: Publications Office of the European Union, 10.2788/9307, 2013.





- Borbon, A., Herve, F., Marc, V., Nadine, L., J.C., G., and Renle, G.: An investigation into the traffic-related fraction of isoprene at an urban location, Atmospheric Environment, 35, 3749–3760, 2001.
- 765 Bressi, M., Sciare, J., Ghersi, V., Bonnaire, N., Nicolas, J. B., Petit, J. E., Moukhtar, S., Rosso, A., Mihalopoulos,
- N., and Féron, A.: A one-year comprehensive chemical characterisation of fine aerosol (PM_{2.5}) at urban,
- suburban and rural background sites in the region of Paris (France), Atmos. Chem. Phys., 13, 7825-7844,
- 768 10.5194/acp-13-7825-2013, 2013.
- 769 Bruns, E. A., Slowik, J. G., El Haddad, I., Kilic, D., Klein, F., Dommen, J., Temime-Roussel, B., Marchand, N.,
- Baltensperger, U., and Prévôt, A. S. H.: Characterization of gas-phase organics using proton transfer reaction
- 771 time-of-flight mass spectrometry: fresh and aged residential wood combustion emissions, Atmospheric
- 772 Chemistry and Physics, 17, 705-720, 10.5194/acp-17-705-2017, 2017.
- 773 Canagaratna, M. R., Jimenez, J. L., Kroll, J. H., Chen, Q., Kessler, S. H., Massoli, P., Hildebrandt Ruiz, L., Fortner,
- 774 E., Williams, L. R., Wilson, K. R., Surratt, J. D., Donahue, N. M., Jayne, J. T., and Worsnop, D. R.: Elemental
- 775 ratio measurements of organic compounds using aerosol mass spectrometry; characterization, improved
- calibration, and implications, Atmospheric Chemistry and Physics, 15, 253-272, 10.5194/acp-15-253-2015,
- 777 2015.
- Canagaratna, M. R., Jayne, J. T., Jimenez, J. L., Allan, J. D., Alfarra, M. R., Zhang, Q., Onasch, T. B., Drewnick,
- F., Coe, H., Middlebrook, A., Delia, A., Williams, L. R., Trimborn, A. M., Northway, M. J., DeCarlo, P. F.,
- 780 Kolb, C. E., Davidovits, P., and Worsnop, D. R.: Chemical and microphysical characterization of ambient
- aerosols with the aerodyne aerosol mass spectrometer, Mass Spectrom Rev, 26, 185-222, 10.1002/mas.20115,
- 782 2007.
- Chakraborty, A., Tripathi, S. N., and Gupta, T.: Effects of organic aerosol loading and fog processing on organic aerosol volatility, Journal of Aerosol Science, 105, 73-83, 10.1016/j.jaerosci.2016.11.015, 2017.
- 785 Chen, G., Canonaco, F., Slowik, J. G., Daellenbach, K. R., Tobler, A., Petit, J. E., Favez, O., Stavroulas, I.,
- 786 Mihalopoulos, N., Gerasopoulos, E., El Haddad, I., Baltensperger, U., and Prevot, A. S. H.: Real-Time Source
- Apportionment of Organic Aerosols in Three European Cities, Environ Sci Technol, 56, 15290-15297,
- 788 10.1021/acs.est.2c02509, 2022a.
- 789 Chen, G., Canonaco, F., Tobler, A., Aas, W., Alastuey, A., Allan, J., Atabakhsh, S., Aurela, M., Baltensperger,
- U., Bougiatioti, A., De Brito, J. F., Ceburnis, D., Chazeau, B., Chebaicheb, H., Daellenbach, K. R., Ehn, M.,
- 791 El Haddad, I., Eleftheriadis, K., Favez, O., Flentje, H., Font, A., Fossum, K., Freney, E., Gini, M., Green, D.
- 792 C., Heikkinen, L., Herrmann, H., Kalogridis, A. C., Keernik, H., Lhotka, R., Lin, C., Lunder, C., Maasikmets,
- 793 M., Manousakas, M. I., Marchand, N., Marin, C., Marmureanu, L., Mihalopoulos, N., Mocnik, G., Necki, J.,
- O'Dowd, C., Ovadnevaite, J., Peter, T., Petit, J. E., Pikridas, M., Matthew Platt, S., Pokorna, P., Poulain, L.,
- Priestman, M., Riffault, V., Rinaldi, M., Rozanski, K., Schwarz, J., Sciare, J., Simon, L., Skiba, A., Slowik, J.
- G., Sosedova, Y., Stavroulas, I., Styszko, K., Teinemaa, E., Timonen, H., Tremper, A., Vasilescu, J., Via, M.,
- Vodicka, P., Wiedensohler, A., Zografou, O., Cruz Minguillon, M., and Prevot, A. S. H.: European aerosol
- 798 phenomenology 8: Harmonised source apportionment of organic aerosol using 22 Year-long ACSM/AMS
- 799 datasets, Environ Int, 166, 107325, 10.1016/j.envint.2022.107325, 2022b.
- Dense Air Quality Sensor Network: https://www.ee.cit.tum.de/esm/projekte/dense-air-quality-sensor-network/,
- last access: 17 October.





- Coggon, M. M., Stockwell, C. E., Claflin, M. S., Pfannerstill, E. Y., Xu, L., Gilman, J. B., Marcantonio, J., Cao,
- 803 C., Bates, K., Gkatzelis, G. I., Lamplugh, A., Katz, E. F., Arata, C., Apel, E. C., Hornbrook, R. S., Piel, F.,
- Majluf, F., Blake, D. R., Wisthaler, A., Canagaratna, M., Lerner, B. M., Goldstein, A. H., Mak, J. E., and
- Warneke, C.: Identifying and correcting interferences to PTR-ToF-MS measurements of isoprene and other
- wrban volatile organic compounds, Atmos. Meas. Tech., 17, 801-825, 10.5194/amt-17-801-2024, 2024.
- 807 Crippa, M., DeCarlo, P. F., Slowik, J. G., Mohr, C., Heringa, M. F., Chirico, R., Poulain, L., Freutel, F., Sciare,
- J., Cozic, J., Di Marco, C. F., Elsasser, M., Nicolas, J. B., Marchand, N., Abidi, E., Wiedensohler, A.,
- Drewnick, F., Schneider, J., Borrmann, S., Nemitz, E., Zimmermann, R., Jaffrezo, J. L., Prévôt, A. S. H., and
- 810 Baltensperger, U.: Wintertime aerosol chemical composition and source apportionment of the organic fraction
- in the metropolitan area of Paris, Atmospheric Chemistry and Physics, 13, 961-981, 10.5194/acp-13-961-2013,
- 812 2013
- Daellenbach, K. R., Kourtchev, I., Vogel, A. L., Bruns, E. A., Jiang, J., Petäjä, T., Jaffrezo, J.-L., Aksoyoglu, S.,
- Kalberer, M., Baltensperger, U., El Haddad, I., and Prévôt, A. S. H.: Impact of anthropogenic and biogenic
- sources on the seasonal variation in the molecular composition of urban organic aerosols: a field and laboratory
- study using ultra-high-resolution mass spectrometry, Atmospheric Chemistry and Physics, 19, 5973-5991,
- 817 10.5194/acp-19-5973-2019, 2019.
- Debevec, C., Sauvage, S., Gros, V., Salameh, T., Sciare, J., Dulac, F., and Locoge, N.: Seasonal variation and
- origins of volatile organic compounds observed during 2 years at a western Mediterranean remote background
- site (Ersa, Cape Corsica), Atmospheric Chemistry and Physics, 21, 1449-1484, 10.5194/acp-21-1449-2021,
- 821 2021.
- Docherty, K. S., Aiken, A. C., Huffman, J. A., Ulbrich, I. M., DeCarlo, P. F., Sueper, D., Worsnop, D. R., Snyder,
- D. C., Peltier, R. E., Weber, R. J., Grover, B. D., Eatough, D. J., Williams, B. J., Goldstein, A. H., Ziemann,
- P. J., and Jimenez, J. L.: The 2005 Study of Organic Aerosols at Riverside (SOAR-1): instrumental
- intercomparisons and fine particle composition, Atmospheric Chemistry and Physics, 11, 12387-12420,
- 826 10.5194/acp-11-12387-2011, 2011.
- 827 Eichler, P., Müller, M., D'Anna, B., and Wisthaler, A.: A novel inlet system for online chemical analysis of semi-
- volatile submicron particulate matter, Atmospheric Measurement Techniques, 8, 1353-1360, 10.5194/amt-8-
- 829 1353-2015, 2015.
- Elser, M., Huang, R.-J., Wolf, R., Slowik, J. G., Wang, Q., Canonaco, F., Li, G., Bozzetti, C., Daellenbach, K. R.,
- Huang, Y., Zhang, R., Li, Z., Cao, J., Baltensperger, U., El-Haddad, I., and Prévôt, A. S. H.: New insights into
- 832 PM2.5 chemical composition and sources in two major cities in China during extreme haze events using
- aerosol mass spectrometry, Atmospheric Chemistry and Physics, 16, 3207-3225, 10.5194/acp-16-3207-2016,
- 834 2016.
- Fleming, L. T., Lin, P., Roberts, J. M., Selimovic, V., Yokelson, R., Laskin, J., Laskin, A., and Nizkorodov, S.
- A.: Molecular composition and photochemical lifetimes of brown carbon chromophores in biomass burning
- organic aerosol, Atmospheric Chemistry and Physics, 20, 1105-1129, 10.5194/acp-20-1105-2020, 2020.
- Freney, E. J., Sellegri, K., Canonaco, F., Boulon, J., Hervo, M., Weigel, R., Pichon, J. M., Colomb, A., Prévôt, A.
- 839 S. H., and Laj, P.: Seasonal variations in aerosol particle composition at the puy-de-Dôme research station in
- France, Atmospheric Chemistry and Physics, 11, 13047-13059, 10.5194/acp-11-13047-2011, 2011.





- Gkatzelis, G. I., Coggon, M. M., McDonald, B. C., Peischl, J., Gilman, J. B., Aikin, K. C., Robinson, M. A.,
- Canonaco, F., Prevot, A. S. H., Trainer, M., and Warneke, C.: Observations Confirm that Volatile Chemical
- Products Are a Major Source of Petrochemical Emissions in U.S. Cities, Environ Sci Technol, 55, 4332-4343,
- 844 10.1021/acs.est.0c05471, 2021.
- Gkatzelis, G. I., Tillmann, R., Hohaus, T., Müller, M., Eichler, P., Xu, K.-M., Schlag, P., Schmitt, S. H., Wegener,
- R., Kaminski, M., Holzinger, R., Wisthaler, A., and Kiendler-Scharr, A.: Comparison of three aerosol
- 847 chemical characterization techniques utilizing PTR-ToF-MS: a study on freshly formed and aged biogenic
- SOA, Atmospheric Measurement Techniques, 11, 1481-1500, 10.5194/amt-11-1481-2018, 2018a.
- Gkatzelis, G. I., Hohaus, T., Tillmann, R., Gensch, I., Müller, M., Eichler, P., Xu, K.-M., Schlag, P., Schmitt, S.
- 850 H., Yu, Z., Wegener, R., Kaminski, M., Holzinger, R., Wisthaler, A., and Kiendler-Scharr, A.: Gas-to-particle
- partitioning of major biogenic oxidation products: a study on freshly formed and aged biogenic SOA,
- Atmospheric Chemistry and Physics, 18, 12969-12989, 10.5194/acp-18-12969-2018, 2018b.
- 6853 Grange, S. K., Fischer, A., Zellweger, C., Alastuey, A., Querol, X., Jaffrezo, J.-L., Weber, S., Uzu, G., and Hueglin,
- 854 C.: Switzerland's PM10 and PM2.5 environmental increments show the importance of non-exhaust emissions,
- 855 Atmospheric Environment: X, 12, 100145, https://doi.org/10.1016/j.aeaoa.2021.100145, 2021.
- 856 Gruber, R. P. and Kalamas, N.: Current Concepts towards the Health Hazards of BBQ Smoke and Newer
- 857 Possibilities for Risk Mitigation: A Pilot Study, Journal of Biomedical Research & Environmental Sciences,
- 5, 675-682, 10.37871/jbres1942, 2024.
- 859 Guo, J., Zhang, J., Shao, J., Chen, T., Bai, K., Sun, Y., Li, N., Wu, J., Li, R., Li, J., Guo, Q., Cohen, J. B., Zhai,
- P., Xu, X., and Hu, F.: A merged continental planetary boundary layer height dataset based on high-resolution
- radiosonde measurements, ERA5 reanalysis, and GLDAS, Earth Syst. Sci. Data, 16, 1-14, 10.5194/essd-16-
- 862 1-2024, 2024.
- Huang, D. D., Zhu, S., An, J., Wang, Q., Qiao, L., Zhou, M., He, X., Ma, Y., Sun, Y., Huang, C., Yu, J. Z., and
- Reference 2864 Zhang, Q.: Comparative Assessment of Cooking Emission Contributions to Urban Organic Aerosol Using
- Online Molecular Tracers and Aerosol Mass Spectrometry Measurements, Environ Sci Technol, 55, 14526-
- 866 14535, 10.1021/acs.est.1c03280, 2021.
- Huang, W., Saathoff, H., Shen, X., Ramisetty, R., Leisner, T., and Mohr, C.: Seasonal characteristics of organic
- aerosol chemical composition and volatility in Stuttgart, Germany, Atmospheric Chemistry and Physics, 19,
- 869 11687-11700, 10.5194/acp-19-11687-2019, 2019.
- Huang, X.-F., Zou, B.-B., He, L.-Y., Hu, M., Prévôt, A. S. H., and Zhang, Y.-H.: Exploration of PM_{2.5} sources on
- the regional scale in the Pearl River Delta based on ME-2 modeling, Atmospheric Chemistry and Physics, 18,
- 872 11563-11580, 10.5194/acp-18-11563-2018, 2018.
- 873 IPCC: Climate Change 2023:Synthesis Report. Contribution of Working Groups I, II and III to the Sixth
- Assessment Report of the Intergovernmental Panel on Climate Change 2023.
- J. L. Jimenez, M. R. Canagaratna, N. M. Donahue, A. S. H. Prevot, Q. Zhang, J. H. Kroll, P. F. DeCarlo, J. D.
- Allan, H. Coe, N. L. Ng, A. C. Aiken, K. S. Docherty, I. M. Ulbrich, and Grieshop, A. P.: Evolution of organic
- aerosols in the atmosphere, Science, 326, 1525-1529, DOI: 10.1126/science.1180353, 2009.
- Jain, V., Tripathi, S. N., Tripathi, N., Sahu, L. K., Gaddamidi, S., Shukla, A. K., Bhattu, D., and Ganguly, D.:
- Seasonal variability and source apportionment of non-methane VOCs using PTR-TOF-MS measurements in
- Belhi, India, Atmospheric Environment, 283, 10.1016/j.atmosenv.2022.119163, 2022.





- Kabir, E., Kim, K. H., Ahn, J. W., Hong, O. F., and Sohn, J. R.: Barbecue charcoal combustion as a potential
- source of aromatic volatile organic compounds and carbonyls, J Hazard Mater, 174, 492-499,
- 883 10.1016/j.jhazmat.2009.09.079, 2010.
- Kajos, M. K., Rantala, P., Hill, M., Hellén, H., Aalto, J., Patokoski, J., Taipale, R., Hoerger, C. C., Reimann, S.,
- and Ruuskanen, T. M.: Ambient measurements of aromatic and oxidized VOCs by PTR-MS and GC-MS:
- intercomparison between four instruments in a boreal forest in Finland, Atmospheric Measurement
- 887 Techniques, 8, 4453-4473, 2015.
- Kim, E., Hopke, P. K., Larson, T. V., Maykut, N. N., and Lewtas, J.: Factor Analysis of Seattle Fine Particles,
- Aerosol Science and Technology, 38, 724-738, 10.1080/02786820490490119, 2004.
- 890 Kodros, J. K., Papanastasiou, D. K., Paglione, M., Masiol, M., Squizzato, S., Florou, K., Skyllakou, K.,
- Kaltsonoudis, C., Nenes, A., and Pandis, S. N.: Rapid dark aging of biomass burning as an overlooked source
- 892 of oxidized organic aerosol, Proc Natl Acad Sci U S A, 117, 33028-33033, 10.1073/pnas.2010365117, 2020.
- Koss, A. R., Sekimoto, K., Gilman, J. B., Selimovic, V., Coggon, M. M., Zarzana, K. J., Yuan, B., Lerner, B. M.,
- Brown, S. S., Jimenez, J. L., Krechmer, J., Roberts, J. M., Warneke, C., Yokelson, R. J., and de Gouw, J.:
- Non-methane organic gas emissions from biomass burning: identification, quantification, and emission factors
- from PTR-ToF during the FIREX 2016 laboratory experiment, Atmospheric Chemistry and Physics, 18, 3299-
- 897 3319, 10.5194/acp-18-3299-2018, 2018.
- Kourtchev, I., Godoi, R. H. M., Connors, S., Levine, J. G., Archibald, A. T., Godoi, A. F. L., Paralovo, S. L.,
- Barbosa, C. G. G., Souza, R. A. F., Manzi, A. O., Seco, R., Sjostedt, S., Park, J.-H., Guenther, A., Kim, S.,
- 900 Smith, J., Martin, S. T., and Kalberer, M.: Molecular composition of organic aerosols in central Amazonia: an
- ultra-high-resolution mass spectrometry study, Atmospheric Chemistry and Physics, 16, 11899-11913,
- 902 10.5194/acp-16-11899-2016, 2016.
- 903 Kumar, B., Chakraborty, A., Tripathi, S. N., and Bhattu, D.: Highly time resolved chemical characterization of
- 904 submicron organic aerosols at a polluted urban location, Environ Sci Process Impacts, 18, 1285-1296,
- 905 10.1039/c6em00392c, 2016.
- 906 Kumar, V., Giannoukos, S., Haslett, S. L., Tong, Y., Singh, A., Bertrand, A., Lee, C. P., Wang, D. S., Bhattu, D.,
- 907 Stefenelli, G., Dave, J. S., Puthussery, J. V., Qi, L., Vats, P., Rai, P., Casotto, R., Satish, R., Mishra, S.,
- Pospisilova, V., Mohr, C., Bell, D. M., Ganguly, D., Verma, V., Rastogi, N., Baltensperger, U., Tripathi, S.
- 909 N., Prévôt, A. S. H., and Slowik, J. G.: Highly time-resolved chemical speciation and source apportionment
- of organic aerosol components in Delhi, India, using extractive electrospray ionization mass spectrometry,
- 911 Atmospheric Chemistry and Physics, 22, 7739-7761, 10.5194/acp-22-7739-2022, 2022.
- 912 Lalchandani, V., Kumar, V., Tobler, A., M. Thamban, N., Mishra, S., Slowik, J. G., Bhattu, D., Rai, P., Satish,
- 913 R., Ganguly, D., Tiwari, S., Rastogi, N., Tiwari, S., Močnik, G., Prévôt, A. S. H., and Tripathi, S. N.: Real-
- time characterization and source apportionment of fine particulate matter in the Delhi megacity area during
- late winter, Science of The Total Environment, 770, 10.1016/j.scitotenv.2021.145324, 2021.
- Lannuque, V., D'Anna, B., Kostenidou, E., Couvidat, F., Martinez-Valiente, A., Eichler, P., Wisthaler, A., Müller,
- 917 M., Temime-Roussel, B., Valorso, R., and Sartelet, K.: Gas-particle partitioning of toluene oxidation products:
- an experimental and modeling study, Atmospheric Chemistry and Physics, 23, 15537-15560, 10.5194/acp-23-
- 919 15537-2023, 2023.





- 920 Leglise, J., Muller, M., Piel, F., Otto, T., and Wisthaler, A.: Bulk Organic Aerosol Analysis by Proton-Transfer-
- 921 Reaction Mass Spectrometry: An Improved Methodology for the Determination of Total Organic Mass, O:C
- 922 and H:C Elemental Ratios, and the Average Molecular Formula, Anal Chem, 91, 12619-12624,
- 923 10.1021/acs.analchem.9b02949, 2019.
- 924 Lemieux, P. M., Lutes, C. C., and Santoianni, D. A.: Emissions of organic air toxics from open burning: a
- comprehensive review, Progress in Energy and Combustion Science, 30, 1-32, 10.1016/j.pecs.2003.08.001,
- 926 2004.
- 927 Lenssen, E. S., Pieters, R. H. H., Nijmeijer, S. M., Oldenwening, M., Meliefste, K., and Hoek, G.: Short-term
- 928 associations between barbecue fumes and respiratory health in young adults, Environ Res, 204, 111868,
- 929 10.1016/j.envres.2021.111868, 2022.
- Li, H., Riva, M., Rantala, P., Heikkinen, L., Daellenbach, K., Krechmer, J. E., Flaud, P.-M., Worsnop, D., Kulmala,
- 931 M., Villenave, E., Perraudin, E., Ehn, M., and Bianchi, F.: Terpenes and their oxidation products in the French
- Landes forest: insights from Vocus PTR-TOF measurements, Atmospheric Chemistry and Physics, 20, 1941-
- 933 1959, 10.5194/acp-20-1941-2020, 2020a.
- Li, S., Liu, D., Wu, Y., Hu, K., Jiang, X., Tian, P., Sheng, J., Pan, B., and Zhao, D.: Aging effects on residential
- 935 biomass burning emissions under quasi-real atmospheric conditions, Environ Pollut, 337, 122615,
- 936 10.1016/j.envpol.2023.122615, 2023.
- 937 Li, W., Wang, J., Qi, L., Yu, W., Nie, D., Shi, S., Gu, C., Ge, X., and Chen, M.: Molecular characterization of
- 938 biomass burning tracer compounds in fine particles in Nanjing, China, Atmospheric Environment, 240,
- 939 10.1016/j.atmosenv.2020.117837, 2020b.
- 940 Liu, T., Wang, Z., Wang, X., and Chan, C. K.: Primary and secondary organic aerosol from heated cooking oil
- 941 emissions, Atmospheric Chemistry and Physics, 18, 11363-11374, 10.5194/acp-18-11363-2018, 2018.
- 942 Malik, T. G., Sahu, L. K., Gupta, M., Mir, B. A., Gajbhiye, T., Dubey, R., Clavijo McCormick, A., and Pandey,
- 943 S. K.: Environmental Factors Affecting Monoterpene Emissions from Terrestrial Vegetation, Plants (Basel),
- 944 12, 10.3390/plants12173146, 2023.
- 945 Massoli, P., Stark, H., Canagaratna, M. R., Krechmer, J. E., Xu, L., Ng, N. L., Mauldin, R. L., Yan, C., Kimmel,
- 946 J., Misztal, P. K., Jimenez, J. L., Jayne, J. T., and Worsnop, D. R.: Ambient Measurements of Highly Oxidized
- Gas-Phase Molecules during the Southern Oxidant and Aerosol Study (SOAS) 2013, ACS Earth and Space
- 948 Chemistry, 2, 653-672, 10.1021/acsearthspacechem.8b00028, 2018.
- 949 Middlebrook, A. M., Bahreini, R., Jimenez, J. L., and Canagaratna, M. R.: Evaluation of Composition-Dependent
- 950 Collection Efficiencies for the Aerodyne Aerosol Mass Spectrometer using Field Data, Aerosol Science and
- 951 Technology, 46, 258-271, 10.1080/02786826.2011.620041, 2012.
- 952 Molteni, U., Bianchi, F., Klein, F., El Haddad, I., Frege, C., Rossi, M. J., Dommen, J., and Baltensperger, U.:
- 953 Formation of highly oxygenated organic molecules from aromatic compounds, Atmospheric Chemistry and
- 954 Physics, 18, 1909-1921, 10.5194/acp-18-1909-2018, 2018.
- 955 Muller, M., Eichler, P., D'Anna, B., Tan, W., and Wisthaler, A.: Direct Sampling and Analysis of Atmospheric
- 956 Particulate Organic Matter by Proton-Transfer-Reaction Mass Spectrometry, Anal Chem, 89, 10889-10897,
- 957 10.1021/acs.analchem.7b02582, 2017.





- 958 Müller, M., Mikoviny, T., Jud, W., D'Anna, B., and Wisthaler, A.: A new software tool for the analysis of high
- 959 resolution PTR-TOF mass spectra, Chemometrics and Intelligent Laboratory Systems, 127, 158-165,
- 960 10.1016/j.chemolab.2013.06.011, 2013.
- 5a62accc9bf9/LHM-StatTB_2023_DS.pdf?utm_source=chatgpt.com, 2023.
- Nakao, S., Clark, C., Tang, P., Sato, K., and Cocker Iii, D.: Secondary organic aerosol formation from phenolic
- compounds in the absence of NOx, Atmospheric Chemistry and Physics, 11, 10649-10660, 10.5194/acp-11-
- 965 10649-2011, 2011.
- 966 Nault, B. A., Jo, D. S., McDonald, B. C., Campuzano-Jost, P., Day, D. A., Hu, W., Schroder, J. C., Allan, J.,
- 967 Blake, D. R., Canagaratna, M. R., Coe, H., Coggon, M. M., DeCarlo, P. F., Diskin, G. S., Dunmore, R., Flocke,
- 968 F., Fried, A., Gilman, J. B., Gkatzelis, G., Hamilton, J. F., Hanisco, T. F., Hayes, P. L., Henze, D. K., Hodzic,
- 969 A., Hopkins, J., Hu, M., Huey, L. G., Jobson, B. T., Kuster, W. C., Lewis, A., Li, M., Liao, J., Nawaz, M. O.,
- 970 Pollack, I. B., Peischl, J., Rappenglück, B., Reeves, C. E., Richter, D., Roberts, J. M., Ryerson, T. B., Shao,
- 971 M., Sommers, J. M., Walega, J., Warneke, C., Weibring, P., Wolfe, G. M., Young, D. E., Yuan, B., Zhang,
- 972 Q., de Gouw, J. A., and Jimenez, J. L.: Secondary organic aerosols from anthropogenic volatile organic
- 973 compounds contribute substantially to air pollution mortality, Atmospheric Chemistry and Physics, 21, 11201-
- 974 11224, 10.5194/acp-21-11201-2021, 2021.
- 975 Niu, Y., Yan, Y., Li, J., Liu, P., Liu, Z., Hu, D., Peng, L., and Wu, J.: Establishment and verification of
- 976 anthropogenic volatile organic compound emission inventory in a typical coal resource-based city, Environ
- 977 Pollut, 288, 117794, 10.1016/j.envpol.2021.117794, 2021.
- 978 Ortega, A. M., Day, D. A., Cubison, M. J., Brune, W. H., Bon, D., de Gouw, J. A., and Jimenez, J. L.: Secondary
- 979 organic aerosol formation and primary organic aerosol oxidation from biomass-burning smoke in a flow
- 980 reactor during FLAME-3, Atmospheric Chemistry and Physics, 13, 11551-11571, 10.5194/acp-13-11551-
- 981 2013, 2013.
- 982 Paatero, P.: The Multilinear Engine—A Table-Driven, Least Squares Program for Solving Multilinear Problems,
- 983 Including then-Way Parallel Factor Analysis Model, Journal of Computational and Graphical Statistics, 8,
- 984 854-888, 10.1080/10618600.1999.10474853, 1999.
- 985 Paatero, P. and Tapper, U.: Positive matrix factorization: A non-negative factor model with optimal utilization of
- 986 error estimates of data values, Environmetrics, 5, 111-126, 10.1002/env.3170050203, 1994.
- 987 Peron, A., Graus, M., Striednig, M., Lamprecht, C., Wohlfahrt, G., and Karl, T.: Deciphering anthropogenic and
- 988 biogenic contributions to selected non-methane volatile organic compound emissions in an urban area,
- 989 Atmospheric Chemistry and Physics, 24, 7063-7083, 10.5194/acp-24-7063-2024, 2024.
- 990 Peter F. DeCarlo, Joel R. Kimmel, Achim Trimborn, Megan J. Northway, John T. Jayne, Allison C. Aiken, Marc
- 991 Gonin, Katrin Fuhrer, Thomas Horvath, Kenneth S. Docherty, Doug R. Worsnop, and Jimenez, J. L.: Field-
- 992 Deployable, High-Resolution, Time-of-FlightAerosol Mass Spectrometer, Analytical Chemistry, 78, 8281-
- 993 8289, 10.1029/2001jd001213, 2006.
- 994 Pfannerstill, E. Y., Wang, N., Edtbauer, A., Bourtsoukidis, E., Crowley, J. N., Dienhart, D., Eger, P. G., Ernle, L.,
- 995 Fischer, H., Hottmann, B., Paris, J.-D., Stönner, C., Tadic, I., Walter, D., Lelieveld, J., and Williams, J.:
- 996 Shipborne measurements of total OH reactivity around the Arabian Peninsula and its role in ozone chemistry,
- 997 Atmospheric Chemistry and Physics, 19, 11501-11523, 10.5194/acp-19-11501-2019, 2019.





- 998 Philippe Dagaut, Zahraa Dbouk , Nesrine Belhadj , Maxence Lailliau , and Benoit, R.: On the combustion of
- 999 terpenes biofuels, ASME Turbo Expo 2024: Turbomachinery Technical Conference and Exposition, London,
- United Kingdom, DOI: 10.1115/GT2024-121549, 2024.
- 1001 Piel, F., Müller, M., Mikoviny, T., Pusede, S. E., and Wisthaler, A.: Airborne measurements of particulate organic
- matter by proton-transfer-reaction mass spectrometry (PTR-MS): a pilot study, Atmospheric Measurement
- Techniques, 12, 5947-5958, 10.5194/amt-12-5947-2019, 2019.
- 1004 Pugliese, G., Piel, F., Trefz, P., Sulzer, P., Schubert, J. K., and Miekisch, W.: Effects of modular ion-funnel
- technology onto analysis of breath VOCs by means of real-time mass spectrometry, Anal Bioanal Chem, 412,
- 7131-7140, 10.1007/s00216-020-02846-8, 2020.
- 1007 Qadir, R. M., Abbaszade, G., Schnelle-Kreis, J., Chow, J. C., and Zimmermann, R.: Concentrations and source
- 1008 contributions of particulate organic matter before and after implementation of a low emission zone in Munich,
- Germany, Environ Pollut, 175, 158-167, 10.1016/j.envpol.2013.01.002, 2013.
- 1010 Qi, L., Vogel, A. L., Esmaeilirad, S., Cao, L., Zheng, J., Jaffrezo, J.-L., Fermo, P., Kasper-Giebl, A., Daellenbach,
- 1011 K. R., Chen, M., Ge, X., Baltensperger, U., Prévôt, A. S. H., and Slowik, J. G.: A 1-year characterization of
- 1012 organic aerosol composition and sources using an extractive electrospray ionization time-of-flight mass
- spectrometer (EESI-TOF), Atmospheric Chemistry and Physics, 20, 7875-7893, 10.5194/acp-20-7875-2020,
- 1014 2020
- 1015 Reizer, M., Calzolai, G., Maciejewska, K., Orza, J. A. G., Carraresi, L., Lucarelli, F., and Juda-Rezler, K.:
- Measurement report: Receptor modeling for source identification of urban fine and coarse particulate matter
- using hourly elemental composition, Atmos. Chem. Phys., 21, 14471-14492, 10.5194/acp-21-14471-2021,
- 1018 2021.
- 1019 Ren, Y., Ge, Y., Gu, B., Min, Y., Tani, A., and Chang, J.: Role of management strategies and environmental
- 1020 factors in determining the emissions of biogenic volatile organic compounds from urban greenspaces, Environ
- 1021 Sci Technol, 48, 6237-6246, 10.1021/es4054434, 2014.
- 1022 Renard, J.-B., Becker, G., Nodorft, M., Tavakoli, E., Thiele, L., Poincelet, E., Scholz, M., and Surcin, J.: High-
- Spatial Resolution Maps of PM2.5 Using Mobile Sensors on Buses: A Case Study of Teltow City, Germany,
- in the Suburb of Berlin, 2023, 10.3390/atmos15121494, 2024.
- 1025 Resler, J., Bauerová, P., Belda, M., Bureš, M., Eben, K., Fuka, V., Geletič, J., Jareš, R., Karel, J., Keder, J., Krč,
- 1026 P., Patiño, W., Radović, J., Řezníček, H., Sühring, M., Šindelářová, A., and Vlček, O.: Challenges of high-
- 1027 fidelity air quality modeling in urban environments PALM sensitivity study during stable conditions,
- 1028 Geoscientific Model Development, 17, 7513-7537, 10.5194/gmd-17-7513-2024, 2024.
- 1029 Reyes-Villegas, E., Green, D. C., Priestman, M., Canonaco, F., Coe, H., Prévôt, A. S. H., and Allan, J. D.: Organic
- 1030 aerosol source apportionment in London 2013 with ME-2: exploring the solution space with annual and
- 1031 seasonal analysis, Atmospheric Chemistry and Physics, 16, 15545-15559, 10.5194/acp-16-15545-2016, 2016.
- Reyes-Villegas, E., Bannan, T., Le Breton, M., Mehra, A., Priestley, M., Percival, C., Coe, H., and Allan, J. D.:
- Online Chemical Characterization of Food-Cooking Organic Aerosols: Implications for Source
- 1034 Apportionment, Environ Sci Technol, 52, 5308-5318, 10.1021/acs.est.7b06278, 2018.
- 1035 Rios, J. C. R.: Atmospheric Chemistry of Isoprene Hydroxyhydroperoxides, The Department of Chemistry and
- 1036 Chemical Biology, Harvard University, 159 pp., 2018.





- 1037 Riva, M., Budisulistiorini, S. H., Chen, Y., Zhang, Z., D'Ambro, E. L., Zhang, X., Gold, A., Turpin, B. J., Thornton,
- 1038 J. A., Canagaratna, M. R., and Surratt, J. D.: Chemical Characterization of Secondary Organic Aerosol from
- Oxidation of Isoprene Hydroxyhydroperoxides, Environ Sci Technol, 50, 9889-9899,
- 1040 10.1021/acs.est.6b02511, 2016.
- Romanias, M. N., Coggon, M. M., Al Ali, F., Burkholder, J. B., Dagaut, P., Decker, Z., Warneke, C., Stockwell,
- 1042 C. E., Roberts, J. M., Tomas, A., Houzel, N., Coeur, C., and Brown, S. S.: Emissions and Atmospheric
- 1043 Chemistry of Furanoids from Biomass Burning: Insights from Laboratory to Atmospheric Observations, ACS
- Earth and Space Chemistry, 8, 857-899, 10.1021/acsearthspacechem.3c00226, 2024.
- 1045 Samad, A., Caballero Arciénega, N. A., Alabdallah, T., and Vogt, U.: Application of the Urban Climate Model
- 1046 PALM-4U to Investigate the Effects of the Diesel Traffic Ban on Air Quality in Stuttgart, Atmosphere, 15,
- 10.3390/atmos15010111, 2024.
- 1048 Schäfer, K., Stefan, E., Stefanie, S., Szabina, T., Balint, A., Janos, O., Mike, P., Christoph, Munkel, Josef Cyrys,
- Annette Peters, and Sarigiannis, D.: A measurement based analysis of the spatial distribution, temporal
- variation and chemical composition of particulate matter in Munich and Augsburg, Int J Tuberc Lung Dis, 20,
- 1051 047-057, 10.5588/ijtld.10.0498, 2011.
- 1052 Schnell, F. I. J.: Aerosol distribution above Munich using remote sensing techniques, Dissertation LMU Munich,
- DOI: 10.5282/edoc.17368, 2014.
- 1054 Schnelle-Kreis J., Istvan Gebefügi, Gerhard Welzl, Thomas Jaensch, and Kettrup, A.: Occurrence of particle-
- associated polycyclic aromatic compounds in ambient air of the city of Munich, Atmospheric Environment,
- 35, S71-S81, https://doi.org/10.1016/S1352-2310(00)00557-4, 2001.
- 1057 Seidler, J., Friedrich, M. N., Thomas, C. K., and Nölscher, A. C.: Introducing the novel concept of cumulative
- 1058 concentration roses for studying the transport of ultrafine particles from an airport to adjacent residential areas,
- 1059 Atmospheric Chemistry and Physics, 24, 137-153, 10.5194/acp-24-137-2024, 2024.
- 1060 Setyan, A., Zhang, Q., Merkel, M., Knighton, W. B., Sun, Y., Song, C., Shilling, J. E., Onasch, T. B., Herndon,
- S. C., Worsnop, D. R., Fast, J. D., Zaveri, R. A., Berg, L. K., Wiedensohler, A., Flowers, B. A., Dubey, M. K.,
- and Subramanian, R.: Characterization of submicron particles influenced by mixed biogenic and
- anthropogenic emissions using high-resolution aerosol mass spectrometry: results from CARES, Atmospheric
- 1064 Chemistry and Physics, 12, 8131-8156, 10.5194/acp-12-8131-2012, 2012.
- 1065 Song, J., Saathoff, H., Jiang, F., Gao, L., Zhang, H., and Leisner, T.: Sources of organic gases and aerosol particles
- and their roles in nighttime particle growth at a rural forested site in southwest Germany, Atmospheric
- 1067 Chemistry and Physics, 24, 6699-6717, 10.5194/acp-24-6699-2024, 2024.
- Song, J., Saathoff, H., Gao, L., Gebhardt, R., Jiang, F., Vallon, M., Bauer, J., Norra, S., and Leisner, T.: Variations
- 1069 of PM2.5 sources in the context of meteorology and seasonality at an urban street canyon in Southwest
- 1070 Germany, Atmospheric Environment, 282, 10.1016/j.atmosenv.2022.119147, 2022.
- 1071 Squires, F. A., Nemitz, E., Langford, B., Wild, O., Drysdale, W. S., Acton, W. J. F., Fu, P., Grimmond, C. S. B.,
- Hamilton, J. F., Hewitt, C. N., Hollaway, M., Kotthaus, S., Lee, J., Metzger, S., Pingintha-Durden, N., Shaw,
- 1073 M., Vaughan, A. R., Wang, X., Wu, R., Zhang, Q., and Zhang, Y.: Measurements of traffic-dominated
- pollutant emissions in a Chinese megacity, Atmospheric Chemistry and Physics, 20, 8737-8761, 10.5194/acp-
- 1075 20-8737-2020, 2020.





- 1076 Srivastava, D., Vu, T. V., Tong, S., Shi, Z., and Harrison, R. M.: Formation of secondary organic aerosols from
- anthropogenic precursors in laboratory studies, npj Climate and Atmospheric Science, 5, 10.1038/s41612-022-
- 1078 00238-6, 2022.
- 1079 Stein, A. F., Draxler, R. R., Rolph, G. D., Stunder, B. J. B., Cohen, M. D., and Ngan, F.: NOAA's HYSPLIT
- 1080 Atmospheric Transport and Dispersion Modeling System, Bulletin of the American Meteorological Society,
- 96, 2059-2077, https://doi.org/10.1175/BAMS-D-14-00110.1, 2015.
- 1082 Stirnberg, R., Cermak, J., Kotthaus, S., Haeffelin, M., Andersen, H., Fuchs, J., Kim, M., Petit, J.-E., and Favez,
- O.: Meteorology-driven variability of air pollution (PM₁) revealed with explainable machine learning,
- 1084 Atmospheric Chemistry and Physics, 21, 3919-3948, 10.5194/acp-21-3919-2021, 2021.
- Ulbrich, I. M., Canagaratna, M. R., Zhang, Q., Worsnop, D. R., and Jimenez, J. L.: Interpretation of organic
- components from Positive Matrix Factorization of aerosol mass spectrometric data, Atmos. Chem. Phys., 9,
- 1087 2891-2918, 10.5194/acp-9-2891-2009, 2009.
- 1088 Vicente, E. D., Vicente, A., Evtyugina, M., Carvalho, R., Tarelho, L. A. C., Oduber, F. I., and Alves, C.:
- Particulate and gaseous emissions from charcoal combustion in barbecue grills, Fuel Processing Technology,
- 1090 176, 296-306, 10.1016/j.fuproc.2018.03.004, 2018.
- Wan, X., Kawamura, K., Ram, K., Kang, S., Loewen, M., Gao, S., Wu, G., Fu, P., Zhang, Y., Bhattarai, H., and
- Cong, Z.: Aromatic acids as biomass-burning tracers in atmospheric aerosols and ice cores: A review, Environ
- Pollut, 247, 216-228, 10.1016/j.envpol.2019.01.028, 2019.
- Wang, L., Slowik, J. G., Tripathi, N., Bhattu, D., Rai, P., Kumar, V., Vats, P., Satish, R., Baltensperger, U.,
- Ganguly, D., Rastogi, N., Sahu, L. K., Tripathi, S. N., and Prévôt, A. S. H.: Source characterization of volatile
- organic compounds measured by proton-transfer-reaction time-of-flight mass spectrometers in Delhi, India,
- 1097 Atmospheric Chemistry and Physics, 20, 9753-9770, 10.5194/acp-20-9753-2020, 2020a.
- 1098 Wang, Q., He, X., Zhou, M., Huang, D. D., Qiao, L., Zhu, S., Ma, Y.-g., Wang, H.-l., Li, L., Huang, C., Huang,
- X. H. H., Xu, W., Worsnop, D., Goldstein, A. H., Guo, H., and Yu, J. Z.: Hourly Measurements of Organic
- 1100 Molecular Markers in Urban Shanghai, China: Primary Organic Aerosol Source Identification and
- Observation of Cooking Aerosol Aging, ACS Earth and Space Chemistry, 4, 1670-1685,
- 10.1021/acsearthspacechem.0c00205, 2020b.
- 1103 Wang, W., Zhang, Y., Jiang, B., Chen, Y., Song, Y., Tang, Y., Dong, C., and Cai, Z.: Molecular characterization
- of organic aerosols in Taiyuan, China: Seasonal variation and source identification, Sci Total Environ, 800,
- 1105 149419, 10.1016/j.scitotenv.2021.149419, 2021.
- Wang, Z., Wang, Z., Sun, J., Wang, Y., Sun, Z., Ma, K., and Wei, L.: Investigation of oxygen-enriched atmosphere
- 1107 combustion of oily sludge: Performance, mechanism, emission of the S/N-containing compound, and residue
- characteristics, Journal of Cleaner Production, 378, 10.1016/j.jclepro.2022.134233, 2022.
- 1109 Wenzel, A., Chen, J., Klama, T., Böhm, F., Angleitner, M., and Lobmaier, R.: Towards high-resolution air
- pollutants sensing through dense low-cost sensor networks a case study in Munich, EGU General Assembly
- 1111 2025, Vienna, Austria, 27 Apr-2 May 2025, https://doi.org/10.5194/egusphere-egu25-16784,
- Williams, L. R., Gonzalez, L. A., Peck, J., Trimborn, D., McInnis, J., Farrar, M. R., Moore, K. D., Jayne, J. T.,
- Robinson, W. A., Lewis, D. K., Onasch, T. B., Canagaratna, M. R., Trimborn, A., Timko, M. T., Magoon, G.,
- Deng, R., Tang, D., de la Rosa Blanco, E., Prévôt, A. S. H., Smith, K. A., and Worsnop, D. R.: Characterization
- of an aerodynamic lens for transmitting particles greater than 1 micrometer in diameter into the Aerodyne





- aerosol mass spectrometer, Atmospheric Measurement Techniques, 6, 3271-3280, 10.5194/amt-6-3271-2013,
- 1117 2013.
- The new 2021 WHO air quality guideline limits.Breeze Technologies Blog.: https://www.breeze-
- technologies.de/blog/new-2021-who-air-quality-guideline-limits/, last access: November 12.
- 1120 Wu, C., Wang, C., Wang, S., Wang, W., Yuan, B., Qi, J., Wang, B., Wang, H., Wang, C., Song, W., Wang, X.,
- 1121 Hu, W., Lou, S., Ye, C., Peng, Y., Wang, Z., Huangfu, Y., Xie, Y., Zhu, M., Zheng, J., Wang, X., Jiang, B.,
- 1122 Zhang, Z., and Shao, M.: Measurement report: Important contributions of oxygenated compounds to emissions
- and chemistry of volatile organic compounds in urban air, Atmospheric Chemistry and Physics, 20, 14769-
- 1124 14785, 10.5194/acp-20-14769-2020, 2020.
- 1125 Wu, T., Müller, T., Wang, N., Byron, J., Langer, S., Williams, J., and Licina, D.: Indoor Emission, Oxidation, and
- New Particle Formation of Personal Care Product Related Volatile Organic Compounds, Environmental
- Science & Technology Letters, 11, 1053-1061, 10.1021/acs.estlett.4c00353, 2024.
- 1128 Xu, C., Chen, J., Zhang, X., Cai, K., Chen, C., and Xu, B.: Emission characteristics and quantitative assessment
- of the health risks of cooking fumes during outdoor barbecuing, Environ Pollut, 323, 121319,
- 1130 10.1016/j.envpol.2023.121319, 2023.
- Ye, Q., Krechmer, J. E., Shutter, J. D., Barber, V. P., Li, Y., Helstrom, E., Franco, L. J., Cox, J. L., Hrdina, A. I.
- 1132 H., Goss, M. B., Tahsini, N., Canagaratna, M., Keutsch, F. N., and Kroll, J. H.: Real-Time Laboratory
- 1133 Measurements of VOC Emissions, Removal Rates, and Byproduct Formation from Consumer-Grade
- Oxidation-Based Air Cleaners, Environmental Science & Technology Letters, 8, 1020-1025,
- 1135 10.1021/acs.estlett.1c00773, 2021.
- 1136 Yee, L. D., Kautzman, K. E., Loza, C. L., Schilling, K. A., Coggon, M. M., Chhabra, P. S., Chan, M. N., Chan,
- 1137 A. W. H., Hersey, S. P., Crounse, J. D., Wennberg, P. O., Flagan, R. C., and Seinfeld, J. H.: Secondary organic
- 1138 aerosol formation from biomass burning intermediates: phenol and methoxyphenols, Atmospheric Chemistry
- and Physics, 13, 8019-8043, 10.5194/acp-13-8019-2013, 2013.
- 1140 Yeoman, A. M., Shaw, M., Carslaw, N., Murrells, T., Passant, N., and Lewis, A. C.: Simplified speciation and
- atmospheric volatile organic compound emission rates from non-aerosol personal care products, Indoor Air,
- 1142 30, 459-472, 10.1111/ina.12652, 2020.
- Zhang, H., Huang, W., Shen, X., Ramisetty, R., Song, J., Kiseleva, O., Holst, C. C., Khan, B., Leisner, T., and
- Saathoff, H.: Aerosol composition, air quality, and boundary layer dynamics in the urban background of
- 1145 Stuttgart in winter, Atmospheric Chemistry and Physics, 24, 10617-10637, 10.5194/acp-24-10617-2024, 2024.
- Zhang, Q., Jimenez Jl Fau Canagaratna, M. R., Canagaratna Mr Fau Ulbrich, I. M., Ulbrich Im Fau Ng, N.
- L., Ng Nl Fau Worsnop, D. R., Worsnop Dr Fau Sun, Y., and Sun, Y.: Understanding atmospheric organic
- aerosols via factor analysis of aerosol mass spectrometry: a review, Anal Bioanal Chem, 401(10), 3045-3067,
- 10.1007/s00216-011-5355-y, 2011.